Journal of
Marine Science and Engineering

MDPI

Article

DNN-MPC Control Based on Two-Layer Optimization Method for the COGAG System

Jingjing Zhang, Jian Li, Xuemin Li * and Xiuzhen Ma

College of Power and Energy Engineering, Harbin Engineering University, 145 Nantong Street, Harbin 150001, China; jingjingzhang@hrbeu.edu.cn (J.Z.); 13804520281@163.com (J.L.); maxiuzhen@hrbeu.edu.cn (X.M.)
* Correspondence: lxm@hrbeu.edu.cn; Tel.: +86-15045077005

Abstract

An engine-propeller cooperative control based on model predictive control (MPC), which takes a deep neural network (DNN) as the prediction model, is studied, and a two-layer optimization method is proposed to improve the economy and maneuverability of the COGAG system. The engine-propeller matching characteristic of the COGAG system is studied, and the economy of the COGAG system is analyzed. In the system planning layer, when the vessel speed command is given, the economic optimal point can be identified. In the local control layer, the DNN-MPC control for different dynamic processes is designed. Moreover, the DNN model has the ability to run in ultra-real time. Compared with parallel control based on PI and parallel power feedback control based on PID, the optimal control based on DNN-MPC can improve the maneuverability of the COGOG pattern by 31.82% and 16.67% in the process of accelerating from 1st to 8th gear and improve the maneuverability of the COGAG pattern by 50% and 23.08% in the process of accelerating from 1st to 10th gear. Moreover, DNN-MPC control can effectively avoid the overshoot of propeller speed caused by the change in pitch adjustment. It provides the theoretical basis for multi-objective optimization of the COGAG system.

Keywords: COGAG system; model predictive control; deep neural network; economy and maneuverability

check for updates

Academic Editor: Simone Mancini

Received: 22 May 2025
Revised: 19 June 2025
Accepted: 24 June 2025
Published: 26 June 2025

Citation: Zhang, J.; Li, J.; Li, X.; Ma, X. DNN-MPC Control Based on Two-Layer Optimization Method for the COGAG System. *J. Mar. Sci. Eng.* **2025**, *13*, 1232. https://doi.org/10.3390/jmse13071232

Copyright: © 2025 by the authors. Licensee MDPI, Basel, Switzerland. This article is an open access article distributed under the terms and conditions of the Creative Commons Attribution (CC BY) license (https://creativecommons.org/licenses/by/4.0/).

1. Introduction

The combined gas turbine and gas turbine (COGAG) system is mainly used to drive large vessels. Due to its large rated power and flexible operating pattern, the system is considered as a potential power device [1,2]. Because there are multiple gas turbines in the system, in the dynamic process the system includes not only single gas turbine control but also cooperative control between different gas turbines. The operation characteristics and control methods of the COGAG system have been extensively studied. Altosole et al. [3] established a complete dynamic model of the COGAG system and studied the operation characteristics of typical dynamic processes. Xie and Wang [4] studied different control strategies for power distribution. On that basis, Li et al. [5] designed a double closed-loop feedback controller for speed and power to achieve the balance of power distribution. Li et al. [6,7] studied the operation characteristics of the COGAG system when the operating pattern is switched under the double closed-loop feedback control. Many studies have focused on the control methods, which can ensure the implementation of complex dynamic processes. However, the steady and dynamic performance of the system has a lot of room for improvement.

In order to improve the maneuverability and ensure the stability of power systems, the switching control method is designed [8–10]. Different optimization algorithms [11,12] (such as genetic algorithms, particle swarm optimization algorithms, and so on) are improved to achieve multi-objective optimal control for power systems, which poses challenges for Lyapunov stability. Due to the competitive relationship among multiple objectives, the optimization effect is very dependent on the weight parameters. Han et al. [13,14] proposed the two-layer control method. In the system planning layer, the optimized control strategy is planned. In the local control layer, the specific control processes are implemented. The advantage of the two-layer control method is that it can separate the optimization objectives in the steady and dynamic processes, which is very suitable for multi-objective optimal control. Economy, maneuverability, and stability are the key performance indicators of vessel propulsion systems [15–17]. Economy can be optimized in the system planning layer, which can ensure that the COGAG system always works at the optimal economic steady-state point. Maneuverability and stability can be optimized in the local control layer, which can shorten the time taken by dynamic processes and ensure the stable operation of the system.

The existing control of the COGAG system for dynamic processes is mainly based on PID [6–8]. The typical feedback control always makes the system response lag behind the external excitation, and it is difficult to make explicit constraints on other variables besides the input. Model predictive control (MPC) is an optimal control algorithm, which is suitable for multi-input systems with constrained requirements [18,19]. With the development of related theories and hardware technologies, MPC has been gradually applied to the control of gas turbine systems [20–24]. In the MPC algorithm, the prediction model is a very important factor, which directly affects the computational efficiency and accuracy of the algorithm [25]. For typical nonlinear systems such as the COGAG system, neural networks and support vector machines are often used to establish the prediction model [26–30]. The prediction sequence cannot be expressed explicitly when the above prediction models are used, so complex and time-consuming solving algorithms are often needed [31–33]. The COGAG system has a short sampling and control period, so the above prediction models may challenge computational efficiency. The linear parameter-varying (LPV) model has the form of a linear model and can well describe nonlinear characteristics [34]. When it is used as the prediction model, the objective function in MPC can be solved explicitly, which can reduce the computational burden greatly. The COGAG system has multiple input variables and a wide operation range. When the LPV model is established for the COGAG system, a large amount of memory space is required to store parameter information about steady-state points and coefficient matrices. Moreover, the model can only apply to the operating region in which the linear model is known. The generalization ability of the model is poor. Yu et al. [35–39] proposed a "two-step" modeling method. By establishing the functional relationship between scheduling parameters and parameters of the LPV model, the generalization ability of the model can be improved. The COGAG system consists of multiple gas turbines and pitch propellers, and there is obvious coupling among the components. The traditional PID-based method controls the gas turbines and pitch propeller independently, which ignores the matching characteristics of the engine and the propeller in the dynamic processes. In the process of a rapid change in working conditions, the phenomenon of propeller speed overshoot often occurs, and there is a large optimization space for maneuverability due to the excessive constraints of transient processes. Aiming at a nonlinear system with many input variables and a large operation range, this paper presents a method combining a two-step modeling method and deep neural network to build the prediction model with an LPV form. Then, the engine-propeller cooperative

control based on MPC is proposed to improve the dynamic response characteristics of the COGAG system.

The remaining content of this paper is arranged as follows: Section 2 describes the structure and establishes the complete nonlinear model of the COGAG system. In Section 3, the ship engine-propeller matching characteristics of the COGAG system are studied, and the economic operation strategy is optimized. In Section 4, the multi-objective optimal control method is described, the deep neural network (DNN) model is established as the prediction model, and the engine-propeller cooperative control is studied. In Section 5, the effectiveness and superiority of the control method are proved. Then, some conclusions are drawn in Section 5.

2. COGAG System

The structure of the port side of the COGAG system is shown in Figure 1. The port and starboard sides of the COGAG system are symmetrical. The port side of the COGAG system is powered by two three-shaft gas turbines. In the three-shaft gas turbine, air is successively compressed by a low-pressure compressor and a high-pressure compressor and enters the combustor. Compressed air is mixed with fuel oil for combustion to generate high-temperature and high-pressure gas. The gas successively expands and does work through the high-pressure turbine, the low-pressure turbine, and the power turbine. The low-pressure and high-pressure turbines provide power to the low-pressure and high-pressure compressors, respectively, through the connecting shaft. The output shaft of the power turbine is connected to the transmission device to provide power to the propeller. In order to meet navigational needs and improve the maneuverability of the vessel, the pitch propeller is generally used as the load. The power turbine is connected to the propeller by necessary shafting and a combined gearbox [2]. The system mainly includes two operating patterns. When the vessel runs slow, a single gas turbine can drive a propeller on each side, which is called the COGOG pattern. When the vessel runs fast, two gas turbines are used to drive a propeller, which is called the COGAG pattern. Based on thermodynamics and dynamics, modules such as the gas turbine and pitch propeller are established, then the COGAG system model is integrated, which is called the complete nonlinear model.

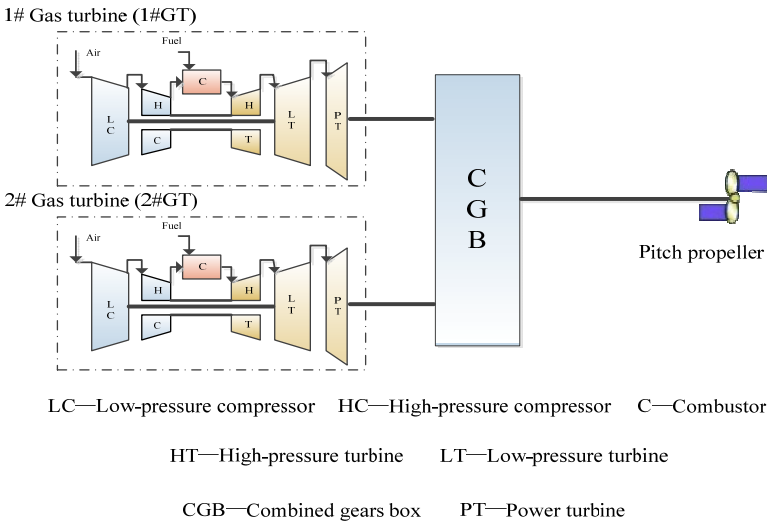


Figure 1. Schematic diagram of the port side of the COGAG system.

2.1. Three-Shaft Gas Turbine

The three-shaft gas turbine mainly includes compressors, a combustion chamber, and turbines. The mathematical models of the different components are as follows.

(1) Compressor

The three-shaft gas turbine consists of a low-pressure compressor and a high-pressure compressor. The characteristics of the compressors are mainly described by four parameters, which are the pressure ratio, reduced flow rate, reduced speed, and efficiency [40]. Once two of the four parameters are determined, the operating state of the compressor can be determined. The compressor characteristics can be calculated as follows:

$$G_c \frac{\sqrt{T_{c,in}}}{P_{c,in}} = f_1\left(\frac{P_{c,out}}{P_{c,in}}, \frac{n_c}{\sqrt{T_{c,in}}}\right) \tag{1}$$

$$\eta_c = f_2\left(\frac{P_{c,out}}{P_{c,in}}, \frac{n_c}{\sqrt{T_{c,in}}}\right) \tag{2}$$

in which G_c denotes compressor the inlet air flow, kg/s; $T_{c,in}$ denotes the compressor inlet air temperature, K; $P_{c,in}$ denotes the compressor inlet pressure, Pa; $P_{c,out}$ denotes the compressor outlet pressure, Pa; n_c denotes the compressor speed, r/min; η_c denotes the compressor efficiency; $G_c \frac{\sqrt{T_{c,in}}}{P_{c,in}}$ denotes the compressor reduced flow rate; $\frac{P_{c,out}}{P_{c,in}}$ denotes the pressure ratio; and $\frac{n_c}{\sqrt{T_{c,in}}}$ denotes the compressor reduced speed.

Considering the specific heat changes in the thermodynamic processes of the compressors, the entropy function [41,42] is used to compute the thermodynamic parameters to improve calculation accuracy.

$$S_{c,out,s} = S_{c,in} + R_g \ln\left(\frac{P_{c,out}}{P_{c,in}}\right) \tag{3}$$

$S_{c,out,s}$ denotes the entropy function of the compressor outlet under adiabatic conditions, and $S_{c,in}$ denotes the entropy function of the compressor inlet. R_g denotes the gas constant, J/(mol·K). The entropy function is only related to temperature, so based on the entropy function of the compressor outlet under adiabatic conditions, the corresponding temperature and specific enthalpy can be obtained.

Compressor power can be expressed as

$$N_c = \frac{G_c(h_{c,out,s} - h_{c,in})}{\eta_c} \tag{4}$$

in which N_c denotes the compressor power, kW; $h_{c,out,s}$ denotes the specific enthalpy of the compressor outlet under adiabatic conditions, J/kg; and $h_{c,in}$ denotes the specific enthalpy of the compressor inlet, J/kg.

(2) Combustion chamber

Based on the conservation of mass, Equation (5) can be obtained:

$$G_{cc,out} = G_{cc,in} + G_f \tag{5}$$

in which $G_{cc,in}$ denotes the air flow at the inlet of the combustion chamber, kg/s; G_f denotes the fuel flow, kg/s; and $G_{cc,out}$ denotes the gas flow at the outlet of the combustion chamber, kg/s.

Based on the conservation of energy, Equation (6) can be obtained:

$$h_{cc,out} = (G_{cc,in} \cdot h_{cc,in} + \eta_B \cdot G_f \cdot H_u)/G_{cc,out} \tag{6}$$

in which $h_{cc,in}$ denotes the specific enthalpy of the combustion chamber inlet, J/kg; η_B denotes the combustion efficiency; H_u denotes the low calorific value of fuel, kJ/kg; and $h_{cc,out}$ denotes the specific enthalpy of the combustion chamber outlet, J/kg.

(3) Turbine

The mathematical model of the turbine is similar to that of the compressor. The characteristics of the turbine are mainly described by the expansion ratio, reduced flow rate, reduced speed, and efficiency. The turbine characteristics can be calculated as follows:

$$G_t \frac{\sqrt{T_{t,in}}}{P_{t,in}} = f_3\left(\frac{P_{t,in}}{P_{t,out}}, \frac{n_t}{\sqrt{T_{t,in}}}\right) \tag{7}$$

$$\eta_t = f_4\left(\frac{P_{t,in}}{P_{t,out}}, \frac{n_t}{\sqrt{T_{t,in}}}\right) \tag{8}$$

in which G_t denotes the turbine inlet gas flow, kg/s; $T_{t,in}$ denotes the turbine inlet gas temperature, K; $P_{t,in}$ denotes the turbine inlet pressure, Pa; $P_{t,out}$ denotes the turbine outlet pressure, Pa; n_t denotes the turbine speed, r/min; and η_t denotes the turbine efficiency.

Turbine power can be expressed as

$$N_t = \frac{G_t(h_{t,in} - h_{t,out,s})}{\eta_t} \tag{9}$$

in which N_t denotes the turbine power, kW; $h_{t,out,s}$ denotes the specific enthalpy of the turbine outlet under adiabatic conditions, J/kg; and $h_{t,in}$ denotes the specific enthalpy of the turbine inlet, J/kg.

The thermal efficiency of the three-shaft gas turbine can be expressed as

$$\eta_g = N_{pt}/(G_f \cdot H_u) \tag{10}$$

in which η_g denotes the thermal efficiency of the gas turbine, and N_{pt} denotes the gas turbine output power, kW.

The compressor is coaxially connected to the turbine. Taking the low-pressure rotor as an example, the rotor differential equation is expressed as follows:

$$\frac{dnl}{dt} = \frac{900(N_{lt}\eta_l - N_{lc})}{nl I_l \pi^2} \tag{11}$$

in which nl denotes the low-pressure compressor speed, r/min; I_l denotes the moment of inertia of the low-pressure rotor, kg·m^2; η_l denotes the low-pressure shaft mechanical efficiency, N_{lt} denotes the low-pressure turbine power, W; and N_{lc} denotes the low-pressure compressor power, W.

2.2. Pitch Propeller

The pitch propeller provides thrust to the vessel by absorbing the kinetic energy provided by the three-shaft gas turbine.

The effective power of the vessel can be expressed as

$$N_S = T_e \cdot V_S \cdot 10^{-3} \tag{12}$$

in which N_S denotes the propeller effective power, kW, and V_S denotes the sailing speed, m/s.

For the COGAG system, the differential equation of propeller speed can be expressed as

$$\frac{dnp}{dt} = \frac{900(N_{pt,1}\eta_s + N_{pt,2}\eta_s - P_s/\eta_d)}{npI_d\pi^2} \tag{13}$$

in which $N_{pt,1}$ denotes the power turbine power of 1#GT, W; $N_{pt,2}$ denotes the power turbine power of 2#GT, W; np denotes the propeller speed, r/min; η_d denotes the propulsive efficiency; η_s denotes the transmission efficiency; and I_d denotes the moment of inertia of the transmission, kg·m^2.

When Equation (13) is balanced, the relationship between N_S and N_{pt} is as follows:

$$N_S = \eta_d \cdot \eta_s \cdot N_{pt} \tag{14}$$

in which $N_{pt} = N_{pt,1} + N_{pt,2}$ denotes the total power of the gas turbines.

By substituting Equation (10) into Equation (14), the relationship between fuel flow and effective power can be obtained:

$$\eta_g \cdot \eta_d \cdot \eta_s = \frac{N_S}{G_f \cdot H_u} \tag{15}$$

Therefore, the economic efficiency of the system η_T can be expressed as

$$\eta_T = \eta_g \cdot \eta_d \cdot \eta_s \tag{16}$$

2.3. Model Validation

The component modules are connected, and the integrated model is solved based on Newton–Rapson and fourth-order Runge–Kutta methods. The simulation values of the gas turbine under rated working conditions are compared with the experimental values [11], as shown in Table 1. Compared with the experimental values, the relative error of the simulation value of each component is within 2.90%, which verifies the accuracy of the system model.

Table 1. Comparison of experimental values and simulation values.

Parameter	Experimental Value	Simulation Value	Relative Error
High-pressure compressor speed (r/min)	9500	9732	2.44%
Low-pressure compressor speed (r/min)	7500	7396	1.38%
Air flow (kg/s)	85.00	83.10	2.23%
Pressure ratio of low-pressure compressor	4.55	4.53	0.43%
Pressure ratio of high-pressure compressor	4.40	4.45	1.14%
Expansion ratio of power turbine	3.45	3.55	2.90%
Power turbine outlet temperature (K)	773.15	775.10	0.25%

3. Methods

3.1. Two-Layer Control Framework

A two-layer control method is designed to optimize the performance of the COGAG system. The schematic diagram of the control method is shown in Figure 2. The system planning layer is used to identify the optimal steady-state point of the system with the goal of economy. The local control layer is responsible for the implementation of control processes, in which maneuverability is optimized under the premise of ensuring stability. We develop the economy optimizing strategy for the system and put the strategy into the system planning layer. When the vessel speed command is given, the optimal operating pattern can be identified, and the target operating point can be guaranteed to be the

economy optimizing point, which is taken as the reference state. In the local control layer, the operation mode is given to the deep neural network (DNN) model to determine the form of the prediction model, and the DNN model for the corresponding pattern is selected as the prediction model. The target speed and pitch ratio can be input into the objective function. The fuel flow of the COGAG system is calculated by solving the quadratic programming problem with constraints online. Then, by collecting parameters such as high-pressure speed, low-pressure speed, power turbine speed, pitch ratio, and fuel flow, the current state of the COGAG system is determined, and the future development trend can be predicted by the DNN model. Based on the rolling optimization mechanism, the fuel flow at the next moment can be calculated. The engine-propeller cooperative control based on DNN-MPC is designed for different dynamic processes.

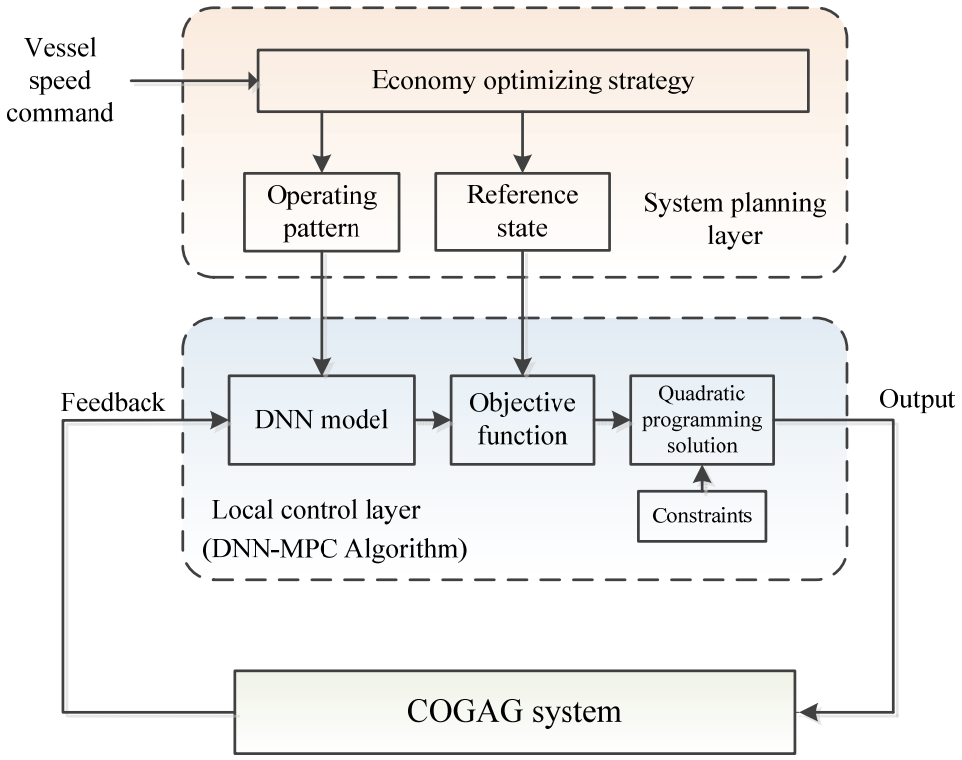


Figure 2. The schematic diagram of the two-layer control.

3.2. Economic Optimization Strategy

Under the premise of ensuring power performance, it is necessary to improve the economy of the COGAG system to reduce fuel consumption. This can not only reduce the use cost of the vessel but also expand the sailing range, which can effectively improve the endurance of the vessel. Fuel consumption per nautical mile g_{Te} is used as the measure of economy, which is defined as follows:

$$g_{Te} = \frac{wf_{total}}{V_s} \tag{17}$$

in which wf_{total} denotes the total fuel flow of the COGAG system, kg/h, and V_S denotes the sailing speed, m/s.

Since the COGAG system includes two operating patterns and uses an adjustable pitch propeller, there are multiple operating points that can provide sufficient power to drive the vessel at a certain speed. We need to find the optimal operating pattern and the corresponding operation point for different working conditions.

Considering different navigation requirements, typical working conditions are divided according to power level, as shown in Table 2. All the data in the paper are normalized.

Table 2. Typical conditions of the COGAG system.

Working Condition	Vessel Speed
1	0.353
2	0.456
3	0.525
4	0.578
5	0.612
6	0.697
7	0.812
8	0.884
9	0.943
10	1

According to the working conditions in Table 1, the system operating points which can meet the corresponding speed conditions and have the best economy need to be found. The optimization objective function can be expressed as follows:

$$\begin{aligned} &\min_{wf_1, wf_2, PR} g_{Te} \\ s.t. \quad &0 < wf_1 \leq 1 \\ &0 < wf_2 \leq 1 \\ &0 < Q \leq 1 \\ &V_{s,tag} - 0.1 < V_s \leq V_{s,tag} + 0.1 \end{aligned} \tag{18}$$

in which wf_1 denotes 1#GT fuel flow, wf_2 denotes 2#GT fuel flow, Q denotes the pitch ratio, and $V_{s,tag}$ denotes the target speed, which is shown in Table 2. The value ranges of the variables in Equation (18) are all normalized.

Equation (18) is solved by using the grid search method based on the steady-state model to obtain the optimal matching operating points for system economy. The optimization process is shown in Figure 3. Firstly, the pitch ratio and propeller speed are initialized. The operating parameters of the COGAG system under the current condition are calculated based on the steady-state model. Then, determine whether the current propeller speed or pitch ratio is greater than the maximum. If not, the propeller speed and pitch ratio are respectively increased at a certain step, then the operating parameters of the updated steady-state point are calculated. Until the two parameters reach the maximum, the operating state at all steady-state points of the COGAG system can be obtained. According to the vessel speed of each working condition in Table 2, the feasible points that meet the speed are selected. The fuel consumption per nautical mile of the feasible points can be compared, then the economical optimal operating point can be selected. The optimization process is carried out for the two operation patterns, so as to formulate the economic optimization operation strategy.

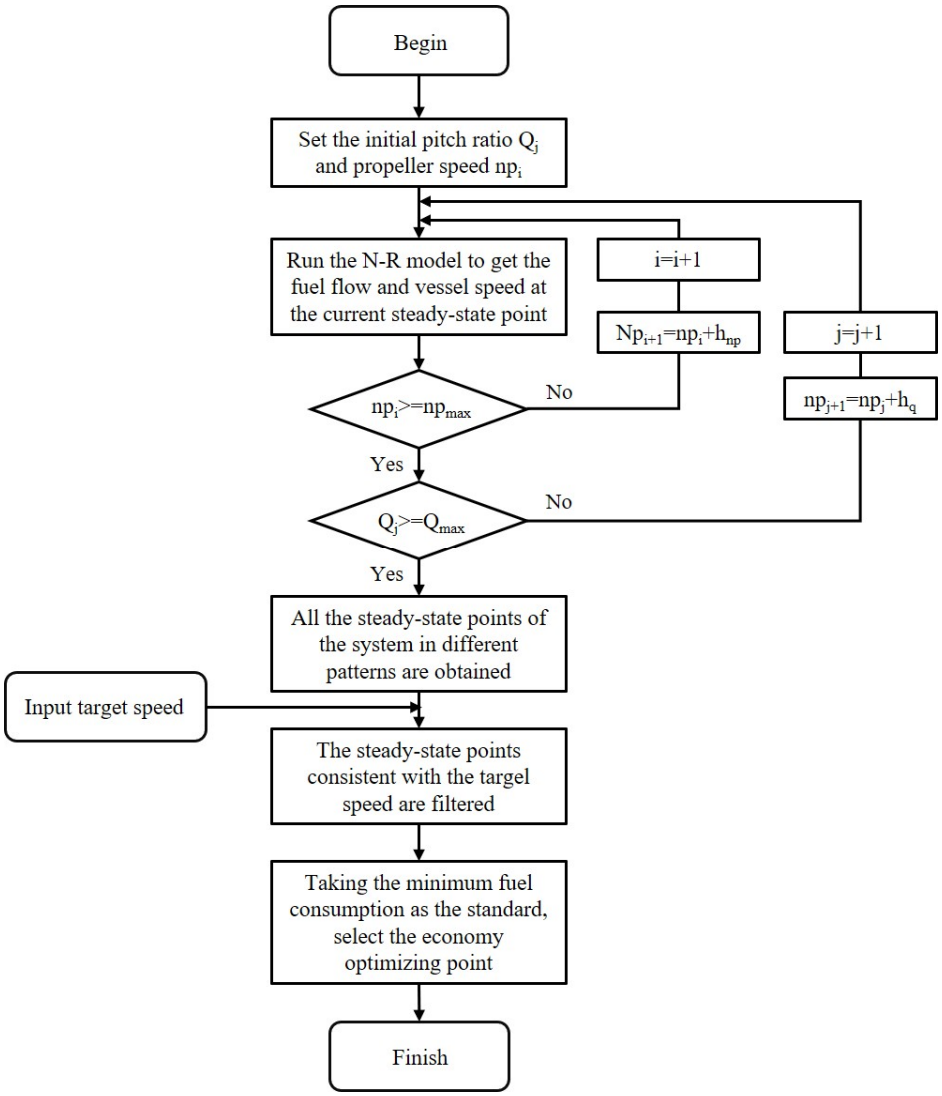


Figure 3. The process of achieving the economic optimization strategy.

The steady-state characteristics of the COGAG pattern at different operating points are shown in Figures 4–8 (PU, Per Unit). Under the same working condition, the effective thrust and effective power of the vessel are uniquely determined. When the system is in working condition 1, the propulsion efficiency increases with the increase in pitch ratio, and the power required by the gas turbine decreases, as shown in Figures 4 and 6. When the pitch ratio is 0.867, the propulsion efficiency reaches the maximum, and the power required by the gas turbine is the minimum. When the working condition is greater than 1 and less than 10, the propulsion efficiency first increases and then decreases, so the gas turbine power first decreases and then increases. When the pitch ratio is 0.9, the propulsion efficiency reaches the maximum, and the power required by the gas turbine is the minimum. At the same working condition, the propeller speed decreases with the increase in pitch ratio. As shown in Figure 5, gas turbine efficiency decreases with the increase in pitch ratio, and gas turbine efficiency increases with the increase in working conditions. As shown in Equation (16), the economic efficiency of the system is determined by both gas turbine efficiency and propulsive efficiency. As shown in Figure 6, the propulsion efficiency at different working conditions is relatively close. The propeller efficiency curves under different working conditions basically overlap. Therefore, for different working conditions, the efficiency of the gas turbine has a greater impact on the total system efficiency.

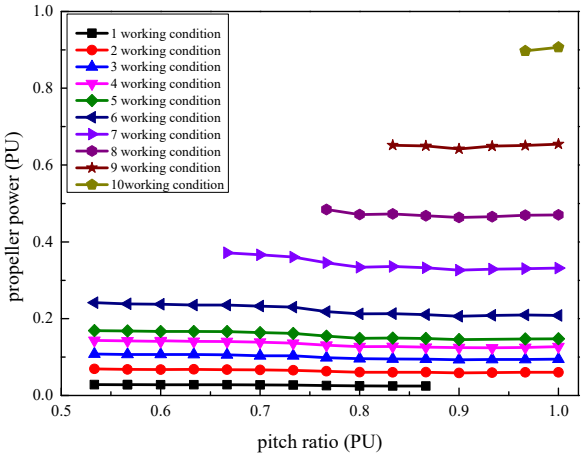


Figure 4. Steady-state characteristics of propeller power in the COGAG pattern.

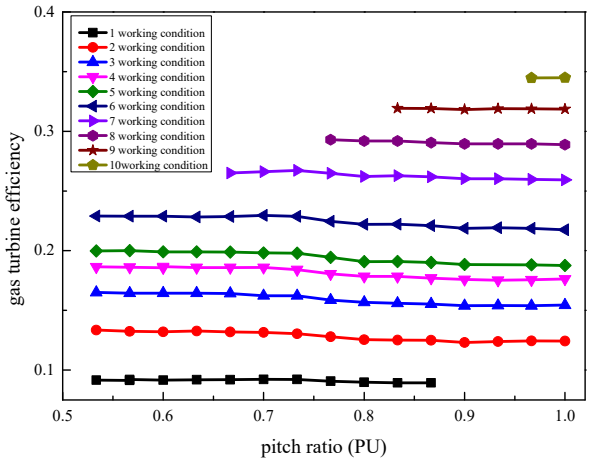


Figure 5. Steady-state characteristics of gas turbine efficiency in the COGAG pattern.

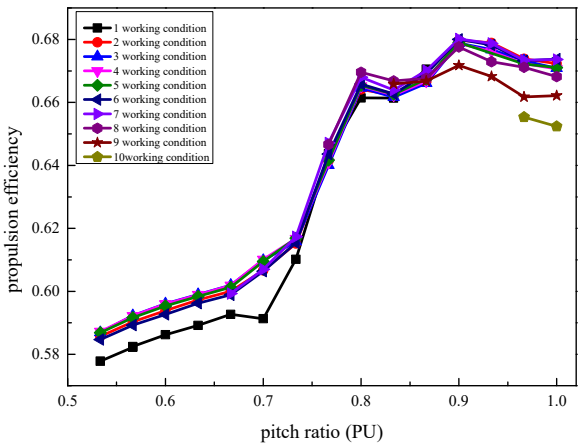


Figure 6. Steady-state characteristics of propulsion efficiency in the COGAG pattern.

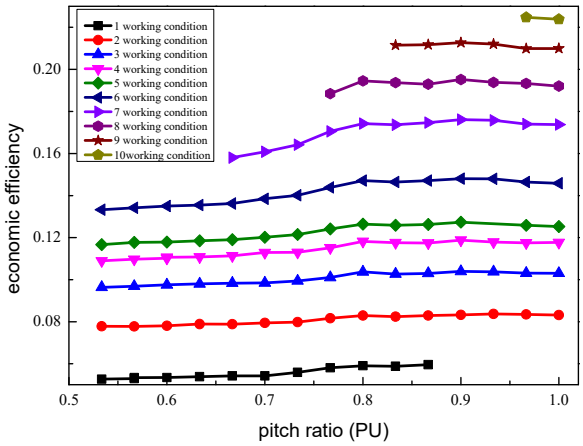


Figure 7. Steady-state characteristics of economic efficiency in the COGAG pattern.

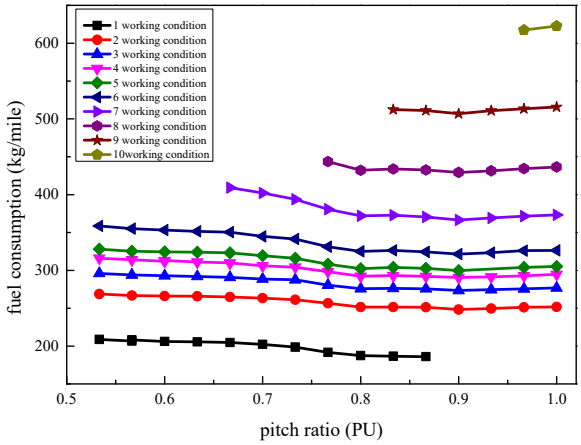


Figure 8. Steady-state characteristics of fuel consumption in the COGAG pattern.

The fuel consumption of the system is determined by the economic efficiency, which means that a higher economic efficiency equates to lower fuel consumption. The characteristics of economic efficiency are similar to propulsion efficiency, indicating that under the same working condition, propulsion efficiency has a greater influence on economic efficiency than gas turbine efficiency.

Based on the above analysis, the economic optimization points of the COGAG pattern under different working conditions can be selected. One of the main functions of the pitch propeller is that the acceleration of the vessel can be achieved by increasing the pitch ratio without changing the fuel flow of the gas turbine. Therefore, when formulating the economic optimization strategy, it is not only necessary to consider the economy but also to ensure that the pitch ratio cannot be reduced when the working condition is increased. Therefore, three economic optimal operating points in each working condition are selected as candidate points firstly, and then the economic optimization operation strategy of the COGAG pattern is formulated by considering the regulation characteristics of the pitch ratio. As the operating state approaches the maximum power of the system, the number of feasible points decreases. At working condition 10, the system economy is optimal when the pitch ratio is 0.967. Frequent adjustment of the pitch during high working conditions switching may lead to the over-rotation of propeller speed, so the pitch ratio should remain unchanged when the working condition is greater than or equal to 9. The economic optimization operation strategy of the COGAG pattern is shown in Table 3. The optimization method of the COGOG pattern is similar, which can meet the power demand of working conditions 1–8.

Table 3. Economic optimization operation strategy of the COGAG pattern.

Working Condition	Pitch Ratio (PU)	Propeller Speed (PU)	Fuel Flow of Single Gas Turbine (kg/s)	Power of Single Gas Turbine (PU)	Economic Efficiency	Fuel Consumption (kg/n mile)
1	0.867	0.342	0.146	0.022	5.96%	186.10
2	0.9	0.437	0.252	0.053	8.33%	248.32
3	0.9	0.508	0.319	0.084	10.39%	273.45
4	0.9	0.560	0.373	0.112	11.88%	290.58
5	0.9	0.590	0.408	0.131	12.73%	299.88
6	0.9	0.667	0.498	0.222	14.80%	321.59
7	0.9	0.777	0.662	0.294	17.61%	366.51
8	0.9	0.862	0.844	0.417	19.52%	429.46
9	0.967	0.902	1.077	0.586	21.00%	513.37
10	0.967	0.984	1.372	0.807	22.47%	617.37

3.3. Optimization Control Method

3.3.1. DNN Prediction Model

The COGAG system is a typical nonlinear system, which has a short sampling period. The linear parameter-varying (LPV) model has the expression form of a linear model and can accurately describe the nonlinear characteristics of the system, which is suitable as the prediction model of the COGAG system. The LPV model of the COGAG system can be described as shown in Equation (19). The steady-state parameters and coefficient matrices in Equation (19) near different steady-state points are different. The relationship between the equations near different steady-state points can be established by scheduling parameter α.

$$\begin{cases} \begin{bmatrix} nl1_{k+1} - nl1_0(\alpha) \\ nh1_{k+1} - nh1_0(\alpha) \\ np_{k+1} - np_0(\alpha) \\ nl2_{k+1} - nl2_0(\alpha) \\ nh2_{k+1} - nh2_0(\alpha) \end{bmatrix} = A \begin{bmatrix} nl1_k - nl1_0(\alpha) \\ nh1_k - nh1_0(\alpha) \\ np_k - np_0(\alpha) \\ nl2_k - nl2_0(\alpha) \\ nh2_k - nh2_0(\alpha) \end{bmatrix} + B \begin{bmatrix} wf1_k - wf1_0(\alpha) \\ wf2_k - wf2_0(\alpha) \\ Q_k - Q_0(\alpha) \end{bmatrix} \\ \begin{bmatrix} N1_k - N1_0(\alpha) \\ N2_k - N2_0(\alpha) \end{bmatrix} = C \begin{bmatrix} nl1_k - nl1_0(\alpha) \\ nh1_k - nh1_0(\alpha) \\ np_k - np_0(\alpha) \\ nl2_k - nl2_0(\alpha) \\ nh2_k - nh2_0(\alpha) \end{bmatrix} + D \begin{bmatrix} wf1_k - wf1_0(\alpha) \\ wf2_k - wf2_0(\alpha) \\ Q_k - Q_0(\alpha) \end{bmatrix} \end{cases} \tag{19}$$

in which $nh1$ denotes the high-pressure compressor speed of 1#GT, $nl1$ denotes the low-pressure compressor speed of 1#GT, $nh2$ denotes the high-pressure compressor speed of 2#GT, $nl2$ denotes the low-pressure compressor speed of 2#GT, np denotes the propeller speed, $N1$ denotes the power of 1#GT, $N2$ denotes the power of 2#GT, $wf1$ denotes the fuel flow of 1#GT, $wf2$ denotes the fuel flow of 2#GT, Q denotes the pitch ratio, subscript '0' denotes the steady-state point, and subscript 'k' denotes the sampling point.

According to Equation (19), the LPV model mainly includes two types of characteristic parameters: steady-state parameters and coefficient matrices. The steady-state parameters are mainly used to describe the steady-state characteristics of the COGAG system, and the coefficient matrices are used to describe the dynamic characteristics of the COGAG system.

Once the parameters of the two parts are determined, the future development trajectory of the COGAG system can be predicted based on the current operating state. According to the characteristics of the LPV model, the steady-state parameters can be identified based on the scheduling parameters, and there is a mapping relationship between steady-state points and coefficient matrices. Therefore, by measuring the scheduling parameters of the dynamic processes, the specific expression of the corresponding LPV model can be determined. The COGAG system has a large number of input variables and a wide range of operation areas. A large number of parameters need to be identified in the LPV model. If the traditional polynomial fitting method is used to identify parameters, the expression form of the polynomial function will be very complicated, and its generalization ability will be poor. As such, the identification accuracy cannot be guaranteed. Therefore, a deep neural network (DNN) model with an LPV form is proposed as the prediction model. The DNN model includes two ANN models in series, which are used for steady-state point and coefficient matrix identification, respectively. The structure diagram of the DNN model is shown in Figure 9. Assume that only the input sequences and the initial state x_t are given. Firstly, the sequences of the scheduling parameters are input into the ANN1 model to identify the steady-state parameters. Then, the measured scheduling parameters and the steady-state parameters predicted by ANN1 are transmitted to the ANN2 model to identify the coefficients of matrices A, B, C, and D. Then, the steady-state parameters and matrix coefficients are put into the LPV model, which is shown in Equation (24), to form the specific expression of the prediction model. By repeatedly inputting the predicted parameters into the DNN model, the development trajectory of the system can be predicted in a long prediction domain. The prediction domain p denotes the predicted step number based on the current parameters. The operation state of the system from $t + 1$ to $t + p$ can be predicted by the DNN model. By switching S from 1 to 2, x_{t+p} is taken as the initial state x_t of the next prediction node. The above process is repeated until the prediction is completed.

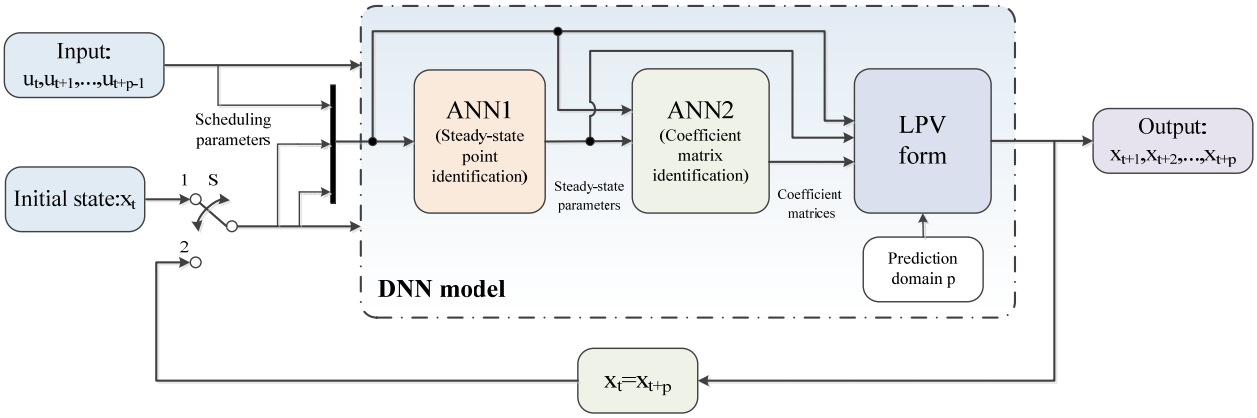


Figure 9. Structure diagram of the DNN model.

(1) Steady-State Point Identification

Take the one-input system as an example; the operation diagram of the one-input system is shown in Figure 10. In the dynamic process, the operating point will deviate from the steady-state operation line due to the dynamic inertia. The operating point can be projected to the steady-state operation line along the X axis or the U axis. Then, the corresponding steady-state point can be determined. Which projection way is adopted depends on the choice of the scheduling parameters. For a multi-input system, the number of scheduling parameters should be the same as the number of input variables. According to Equation (24), the COGAG system has three input variables, so three scheduling parameters

are required to identify the corresponding steady-state point. Considering that both gas turbines can affect the operating state of the system, it is necessary to select one parameter from each of the two gas turbines. For a three-shaft gas turbine, the operation state can be identified based on the high-pressure compressor speed, low-pressure compressor speed, or power turbine speed [43]. Since the power turbines of the two gas turbines are both connected to the propeller through the transmission device, power turbine speed is not suitable as the scheduling parameter. Therefore, $nh1$ and $nh2$ are selected as the scheduling parameters in this paper. In addition, the working state of the pitch propeller is required. PR is taken as the third scheduling parameter. Therefore, the steady-state point can be determined by $nh1$, $nh2$, and PR; then, the steady-state parameters can be obtained, including $wf1$, $wf2$, $nl1$, $nl2$, np, $N1$, and $N2$.

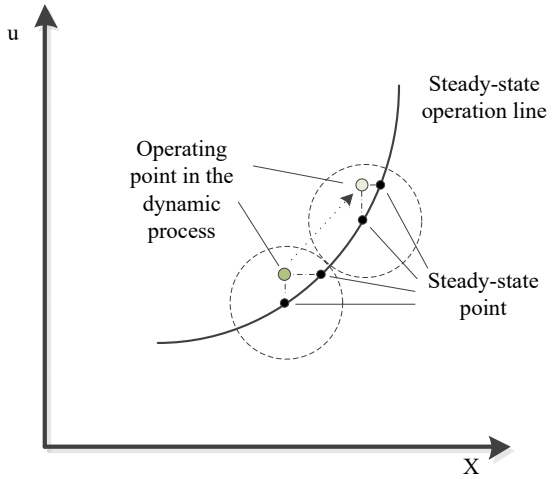


Figure 10. One-input system operation diagram.

The following steps are carried out to establish the steady-state identification model:

1. Based on the steady-state model, steady-state point parameters can be obtained, including Q, $wf1$, $wf2$, $nl1$, $nh1$, $nl2$, $nh2$, np, $N1$, and $N2$, which is taken as the data set.
2. Standardize the data and divide it into a training set and test set. Calculate the mean value and variance of the data and standardize the data according to Equation (20). Eighty percent of the data set is randomly divided into the training set with the remaining twenty percent comprising the test set.

$$x_{data,s} = \frac{x_{data} - \overline{x}}{v} \tag{20}$$

in which $\overline{x}$ denotes the mean value of x_{data}, and v denotes the variance of x_{data}.

3. The artificial neural network (ANN) model, which is used to identify steady-state points, is established. ANN1 is a dense connection layer neural network. $x_{ann,t} = [PR_t,\ nh1_t,\ nh2_t]$ is taken as the input, and $y_{ann,t} = [wf1,\ wf2,\ nl1,\ nl2,\ np, N1, N2]$ is taken as the output. The hyperparameters are optimized, and the model is trained by a back propagation algorithm. The parameters of the ANN1 model are shown in Table 4.
4. Verify the accuracy of the model based on the test set and save the model.

Table 4. The parameters of the ANN1 model.

Parameter	COGAG Pattern	COGOG Pattern
Number of network layers	3	3
Neuron distribution	(120, 240, 120)	(120, 120, 120)
Activation function	relu	relu
Loss function	MSE	MSE
Epochs	3000	1500
Learning rate	0.0005	0.001
Optimizer	Nadam	Adam
Training MSE	1.91×10^{-4}	1.29×10^{-4}
Test MSE	3.87×10^{-4}	1.88×10^{-4}

The mean square error (MSE) of the training set in the COGAG pattern is 1.91×10^{-4}. The MSE of the test set in the COGAG pattern is 3.87×10^{-4}. The MSE of the training set in the COGOG pattern is 1.29×10^{-4}. The MSE of the test set in the COGOG pattern is 1.88×10^{-4}.

(2) Coefficient Matrix Identification

The dynamic characteristics of the LPV model are described by the coefficient matrices. The operating principle of the COGAG system is complex, so it is difficult to obtain the exact explicit expression of the coefficient matrices. In this paper, the small deviation linearization method is adopted to obtain the coefficient matrices near different steady-state points. Firstly, make a small step of each input variable in turn at the steady-state point, and the data based on the complete nonlinear model in the dynamic process can be obtained. Then, the least square fitting technique is carried out by using the SCIPY module in the Python 3.9 environment to obtain the corresponding coefficient matrices, as shown in Equation (21). The above process is repeated at different steady-state points to obtain the data set of the coefficient matrices.

$$\begin{bmatrix} A & B \\ C & D \end{bmatrix} = min\sum_{k=1}^{K} \left\| \begin{bmatrix} nl1_{k+1} - nl1_0 \\ nh1_{k+1} - nh1_0 \\ np_{k+1} - np_0 \\ nl2_{k+1} - nl2_0 \\ nh2_{k+1} - nh2_0 \\ N1_k - N1_0 \\ N2_k - N2_0 \end{bmatrix} - \begin{bmatrix} A & B \\ C & D \end{bmatrix} \begin{bmatrix} nl1_k - nl1_0 \\ nh1_k - nh1_0 \\ np_k - np_0 \\ nl2_k - nl2_0 \\ nh2_k - nh2_0 \\ wf1_k - wf1_0 \\ wf2_k - wf2_0 \\ Q_k - Q_0 \end{bmatrix} \right\|_2 \quad (21)$$

in which K denotes the sampling number in the dynamic process.

After the data set is obtained, an artificial neural network (ANN) model is also used to predict the coefficient matrices. The schematic diagram of ANN2 is shown in Figure 11. According to Equation (19), a large number of matrix coefficients need to be identified. If the traditional dense connected layer structure is adopted, it is assumed that there is a coupling relationship among the elements of different coefficient matrices. However, since the elements in a coefficient matrix are obtained by fitting, there is no obvious relationship among them. In order to improve the accuracy of coefficient prediction, the ANN2 model is divided into modules to ensure that the identification process of each parameter is independent.

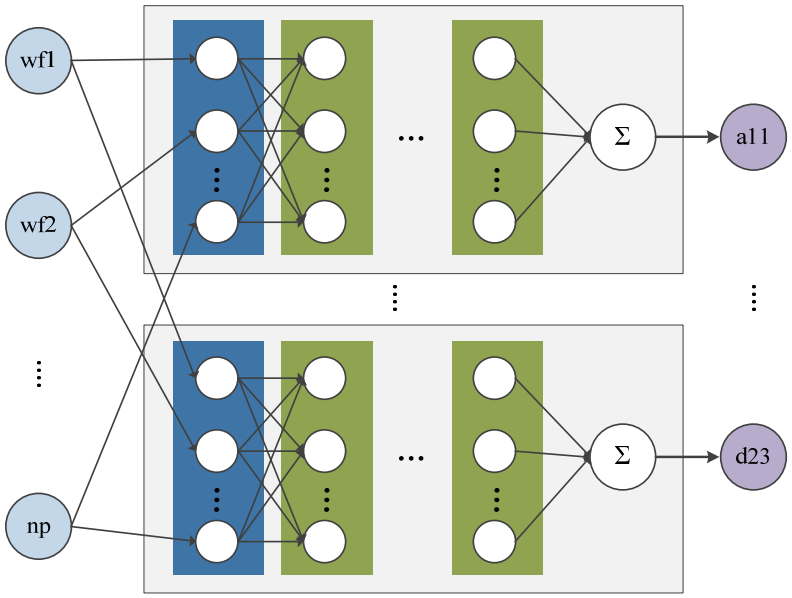


Figure 11. The schematic diagram of ANN2.

The process of establishing the coefficient matrix identification model is similar to that of the steady-state identification model. Q, $nh1$, $nh2$, $wf1$, $wf2$, $nl1$, $nl2$, and np are taken as the input. The coefficients of matrices A, B, C, and D are taken as the output. The parameters of the ANN2 model are shown in Table 5.

Table 5. The parameters of the ANN2 model.

Parameter	COGAG Pattern	COGOG Pattern
Number of network layers	3	3
Neuron distribution	(2640, 2640, 2640)	(1200, 1200, 1200)
Activation function	relu	relu
Loss function	MSE	MSE
Epochs	3000	3000
Learning rate	0.0002	0.0002
Optimizer	Adam	Adam
Training MSE	8.27×10^{-3}	3.9×10^{-3}
Test MSE	6.68×10^{-2}	1.38×10^{-2}

The MSE of the training set in the COGAG pattern is 8.27×10^{-3}. The MSE of the test set in the COGAG pattern is 6.68×10^{-2}. The MSE of the training set in the COGOG pattern is 3.9×10^{-3}. The MSE of the test set in the COGOG pattern is 1.38×10^{-2}.

(3) DNN Model Validation

The accuracy of the DNN model under the COGAG pattern is verified. The dynamic characteristics of the DNN model and the complete nonlinear model are shown in Figures 12–16. The dynamic response of the DNN model is consistent with that of the complete nonlinear model. In the whole dynamic process, compared with the complete nonlinear model, the MRE of the 1#GT low-pressure compressor speed of the DNN model is 0.28%, the MRE of the 1#GT high-pressure compressor speed is 0.11%, the MRE of the 2#GT low-pressure compressor speed of the DNN model is 0.25%, the MRE of the 2#GT high-pressure compressor speed is 0.10%, and the MRE of the propeller speed is 0.43%. In terms of accuracy, the DNN model can be entirely equivalent to the complete nonlinear model based on the working principle. In addition, the calculation time of the DNN model

is about 16.8 ms in a single calculation cycle, which can achieve ultra-real-time operation and can be used as an online prediction model.

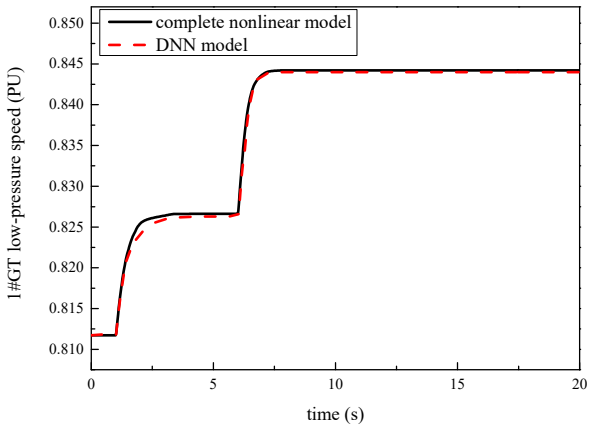


Figure 12. Low-pressure compressor speed of 1#GT.

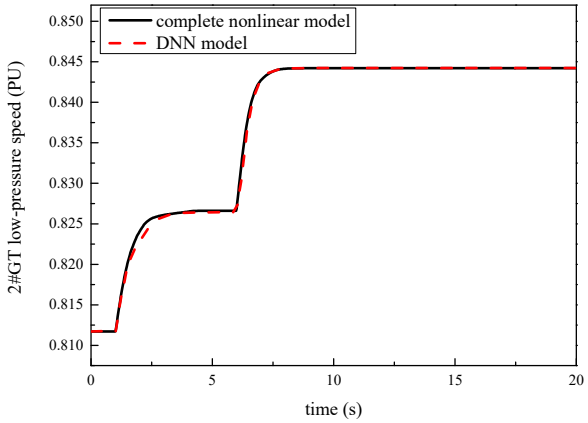


Figure 13. Low-pressure compressor speed of 2#GT.

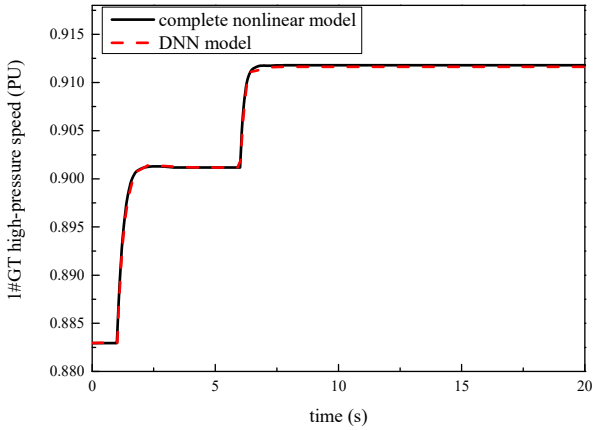


Figure 14. High-pressure compressor speed of 1#GT.

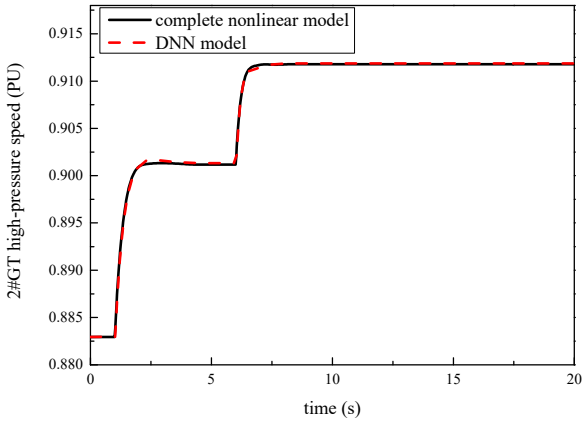


Figure 15. High-pressure compressor speed of 2#GT.

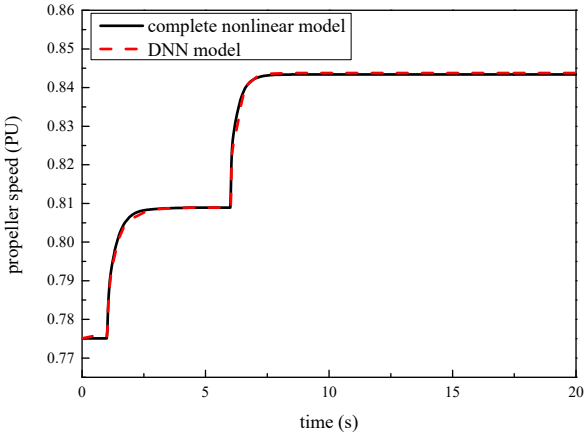


Figure 16. Propeller speed.

3.3.2. Engine-Propeller Cooperative Control

For the COGAG system, the existing method controls pitch ratio and fuel separately, which ignores the engine-propeller matching characteristics so that the propeller speed will significantly drop and overshoot in the dynamic processes. Therefore, model predictive control (MPC) for different dynamic processes is studied. The regulation characteristics of pitch ratio are input into MPC, then the system response performance under the pitch regulation can be predicted by the prediction model, and MPC control of the fuel flow of the gas turbine is carried out.

Model predictive control (MPC) is a model-based control method [44,45]. MPC can identify the current operating state and predict the future trajectory of the system based on the prediction model. In order to make the predicted trajectory as close as possible to the target trajectory, the optimization objective function is established. The optimal input of the system can be obtained by solving the objective function.

The objective functions for different dynamic processes are different. In this paper, the objective functions for three typical dynamic processes, which include speed control in the COGOG pattern and power distribution control and speed control in the COGAG pattern, are designed.

The objective function for speed control in the COGOG pattern is as follows:

$$min J_1(\Delta U_{in}(k)) = \left\| \Gamma_y \left(Y_{np}(k) - np_{tag} \right) \right\|^2 + \| \Gamma_u \Delta U_{in}(k) \|^2 \quad (22)$$

in which np_{tag} denotes the target propeller speed sequence, $Y_{np}(k)$ denotes the predicted propeller speed sequence, $\Delta U_{in}(k)$ denotes the input increment to be solved, and Γ_y and Γ_u denote weight matrices.

The objective function for power distribution control is as follows:

$$minJ_2(\ \Delta U_{in}(k)) = \left\|\Gamma_y\left(Y_p(k) - P_{tag}\right)\right\|^2 + \left\|\Gamma_u \Delta U_{in}(k)\right\|^2 \tag{23}$$

in which P_{tag} denotes the target power sequence, and $Y_p(k)$ denotes the predicted power sequence.

The objective function for speed control in the COGAG pattern is as follows:

$$minJ_3(\ \Delta U_{in}(k)) = \left\|\Gamma_y\left(Y_{np}(k) - np_{tag}\right)\right\|^2 + \left\|\Gamma_u \Delta U_{in}(k)\right\|^2 + \left|\left|\Gamma_p(P_1(k) - P_2(k))\right|\right|^2 \tag{24}$$

In order to ensure the power balance of the two gas turbines, a penalty term is added to the objective function in which $P_1(k)$ denotes 1#GT predicted power, $P_2(k)$ denotes 2#GT predicted power, and Γ_p denotes the penalty weight matrix.

Then, the detailed derivation process for speed control in the COGAG pattern will be described. The other two derivation processes are similar.

Equation (19) can be simplified as follows:

$$\begin{cases} x_{k+1} - x_0 = A(x_k - x_0) + B(u_k - u_0) \\ y_k - y_0 = C(x_k - x_0) + D(u_k - u_0) \end{cases} \tag{25}$$

in which $u = [wf1, wf2, PR]^T$, $x = [nl1, nh1, np, nl2, nh2]^T$, and $y = [N1, N2]^T$.

The relation of adjacent moments can be obtained by subtraction:

$$x_{k+1} - x_k = A(x_k - x_{k-1}) + B(u_k - u_{k-1}) \tag{26}$$

$$y_{k+1} - y_k = C(x_{k+1} - x_k) + D(u_{k+1} - u_k) \tag{27}$$

Simplifying Equations (26) and (27), the following equations can be obtained:

$$\Delta x_{k+1} = A\Delta x_k + B\Delta u_k \tag{28}$$

$$\Delta y_{k+1} = C\Delta x_{k+1} + D\Delta u_k \tag{29}$$

in which $\Delta x_k = x_k - x_{k-1}$, $\Delta u_k = u_k - u_{k-1}$, and $\Delta y_{k+1} = y_{k+1} - y_k$.

Equation (30) can be obtained by recursion:

$$x_{k+2} - x_k = \left(A^2 + A\right)\Delta x_k + (A + I)B\Delta u_k + B\Delta u_{k+1} \tag{30}$$

$$\begin{aligned} x_{k+p} - x_k = (A^p + \cdots + A)\Delta x_k + \left(A^{p-1} + \cdots + I\right)B\Delta u_k + \cdots \\ +(A^{p-m} + \cdots + I)B\Delta u_{k+m} \end{aligned}$$

in which p denotes the prediction domain, and m denotes the control domain.

Substitute Equation (28) into Equation (29):

$$\Delta y_{k+1} = CA\Delta x_k + CB\Delta u_k + D\Delta u_{k+1} \tag{31}$$

The following can be obtained by recursion:

$$y_{k+2} - y_k = C\left(A^2 + A\right)\Delta x_k + C(A + I)B\Delta u_k + (CB + D)\Delta u_{k+1} + D\Delta u_{k+2} \tag{32}$$

$$y_{k+p} - y_k = C\left(A^p + A^{p-1} + \cdots + A\right)\Delta x_k + C\left(A^{p-1} + A^{p-2} + \cdots + A + I\right)B\Delta u_k + \cdots + (C(A^{p-m} + \cdots + I)B + D)\Delta u_{k+m}$$

Equation (32) can be expressed in matrix form as follows:

$$\begin{aligned} Y(k+1|k) = & \begin{bmatrix} E \\ E \\ \vdots \\ E \end{bmatrix} y_k + \begin{bmatrix} CA \\ C\left(A^2 + A\right) \\ \vdots \\ C(A^p + \cdots + A) \end{bmatrix} \Delta x_k \\ & + \begin{bmatrix} CB & \cdots & 0 \\ \vdots & \ddots & \vdots \\ CB\left(A^{p-1} + \cdots + I\right) & \cdots & CB(A^{p-m} + \cdots + I) + D \end{bmatrix} \begin{bmatrix} \Delta u_k \\ \Delta u_{k+1} \\ \vdots \\ \Delta u_{k+m} \end{bmatrix} \end{aligned} \tag{33}$$

in which $Y(k+1|k) = \left[y_{k+1}, y_{k+2}, \ldots, y_{k+p}\right]^T$.

Equation (33) can be simplified as follows:

$$Y(k+1|k) = S_x \Delta x(k) + \tau y_k + S_u \Delta U(k) \tag{34}$$

in which $S_x = \begin{bmatrix} CA \\ C\left(A^2 + A\right) \\ \vdots \\ \sum_{i=1}^{p} CA^i \end{bmatrix}_{p\times 1}$, $E = \begin{bmatrix} 1 \\ 1 \\ \vdots \\ 1 \end{bmatrix}_{yn\times 1}$, $\tau = \begin{bmatrix} E \\ E \\ \vdots \\ E \end{bmatrix}_{p\times 1}$, $\Delta U(k) = \begin{bmatrix} \Delta u_k \\ \Delta u_{k+1} \\ \vdots \\ \Delta u_{k+m-1} \end{bmatrix}_{m\times 1}$,

$S_u = \begin{bmatrix} CB & 0 & \cdots & 0 \\ CAB + CB & CB & \cdots & \vdots \\ \vdots & \vdots & \vdots & CB \\ \sum_{i=1}^{p} CA^{i-1}B & \sum_{i=1}^{p} CA^{i-1}B & \cdots & \sum_{i=1}^{p-m+1} CA^{i-1}B \end{bmatrix}_{p\times m}$, and yn denotes the number of predicted output variables.

In the process of speed control, the pitch ratio is controlled by an open loop, and the fuel flow is controlled by MPC. Therefore, we need to divide $\Delta U(k) = [wf1,\ wf2,\ Q]^T$ into $\Delta U_1(k) = [wf1,\ wf2]^T$ and $\Delta U_2(k) = Q$. $\Delta U_1(k)$ is the $\Delta U_{in}(k)$ in Equation (24). By adding the pitch control law to the objective function, the prediction model can predict the response performance under the pitch ratio adjustment so that the engine-propeller cooperative control can be carried out. Meanwhile, we also need to extract the corresponding columns from the S_u matrix. S_u can be divided into S_{u1} and S_{u2}. Equation (37) can be expressed as follows:

$$Y(k+1|k) = S_x \Delta x(k) + \tau y_k + S_{u1} \Delta U_1(k) + S_{u2} \Delta U_2(k) \tag{35}$$

Equation (35) is the general expression of the prediction sequence. According to Equation (24), we should obtain the special expressions of $Y_{np}(k)$, $P_1(k)$, and $P_2(k)$. When $Y(k+1|k) = Y_{np}(k)$, C is $[0\ 0\ 1\ 0\ 0]$, and D is $[0\ 0\ 0]$. When $Y(k+1|k) = P_1(k)$, C is $[C_{11}\quad C_{12}\quad C_{13}\quad 0\quad 0\ ]$, and D is $[D_{11}\quad D_{12}\quad D_{13}]$. When $Y(k+1|k) = P_2(k)$, C is $[0\quad 0\quad C_{23}\quad C_{24}\quad C_{25}\ ]$, and D is $[D_{21}\quad D_{22}\quad D_{23}]$. $Y_{np}(k)$, $P_1(k)$, and $P_2(k)$ can be expressed as follows:

$$Y_{np}(k) = S_{x,np} \Delta x(k) + \tau np_k + S_{u1,np} \Delta U_1(k) + S_{u2,np} \Delta U_2(k) \tag{36}$$

$$P_1(k) = S_{x,p1} \Delta x(k) + \tau N1_k + S_{u1,p1} \Delta U_1(k) + S_{u2,p1} \Delta U_2(k) \tag{37}$$

$$P_2(k) = S_{x,p2}\Delta x(k) + \tau N2_k + S_{u1,p2}\Delta U_1(k) + S_{u2,p2}\Delta U_2(k) \tag{38}$$

Put Equations (36)–(38) into Equation (24) and simplify Equation (24) into the quadratic programming (QP):

$$J_3(\Delta U_1(k)) = \frac{1}{2}\Delta U_1(k)^T H \Delta U_1(k) + G(k+1|k)^T \Delta U_1(k) \tag{39}$$

in which $H = 2(S_{u1,np}^T \Gamma_y^T \Gamma_y S_{u1,np} + \Gamma_u^T \Gamma_u + M^T \Gamma_p^T \Gamma_p M)$, $G(k+1|k) = 2(M^T \Gamma_p^T \Gamma_p E_N(k+1|k) - S_{u1,np}^T \Gamma_y^T \Gamma_y E_{np}(k+1|k))$, $M = S_{u1,p1} - S_{u1,p2}$, $E_{np}(k+1|k) = np_{tag} - S_{x,np}\Delta x(k) - \tau np_k - S_{u2,np}\Delta U_2(k)$, and $E_N(k+1|k) = \tau(N1_k - N2_k) + (S_{x,p1} - S_{x,p2})\Delta x(k) + (S_{u2,p1} - S_{u2,p2})\Delta U_2(k)$.

In the dynamic process, it is necessary to ensure the security and stability of the COGAG system. Based on the analysis of the operating characteristics of the COGAG system, stable operation can be guaranteed when the propeller speed and fuel flow are constrained [41]. The corresponding constraints can be expressed as follows:

$$U_{1,min} - U_{1,k-1} \le \Delta U_1(k) \le U_{1,max} - U_{1,k-1} \tag{40}$$

$$Y_{np,min} \le Y_{np}(k) \le Y_{np,max} \tag{41}$$

in which $U_{1,min}$ denotes the minimum fuel flow, $U_{1,max}$ denotes the maximum fuel flow, $Y_{np,min}$ denotes the minimum propeller speed, and $Y_{np,max}$ denotes the maximum propeller speed.

When the system works in COGAG pattern, the power balance of the two gas turbines is also an important indicator of stability. This is achieved by adding a power difference penalty term to the objective function, which is shown in Equation (24). The objective function with constraints is shown in Equation (42).

$$\min_{\Delta U_1} \frac{1}{2}\Delta U_1(k)^T H \Delta U_1(k) + G(k+1|k)^T \Delta U_1(k) \tag{42}$$

$$s.t. \quad l \le C_u \Delta U_1(k) \le h$$

in which $C_u = [I, S_{u1,np}]^T$, $l = [U_{1,min} - U_{1,k-1}, Y_{np,min} - S_{x,np}\Delta x(k) - \tau np_k - S_{u2,np}\Delta U_2(k)]^T$, and $h = [U_{1,max} - U_{1,k-1}, Y_{np,max} - S_{x,np}\Delta x(k) - \tau np_k - S_{u2,np}\Delta U_2(k)]^T$. The simplified dual neural network can be used to solve Equation (42) to improve computing efficiency [46, 47].

4. Results and Discussion

4.1. Speed Control in the COGOG Pattern

The acceleration process of the COGAG system under the COGOG pattern from working conditions 1 to 8 is simulated. The operating conditions are as follows. In the first 2 s, the system runs at working condition 1. At 2 s, the acceleration command is given to accelerate the system to working condition 8. The simulation finishes at 120 s. The parallel control based on PI is mainly used in current engineering practice. On that basis, a parallel power feedback control based on PID is proposed in the existing reports. Therefore, the engine-propeller cooperative control based on DNN-MPC is compared with the above two control methods. Set the weight factor of MPC to $\Gamma_{y,n}$ = 0.78, and $\Gamma_{u,n}$ = 0.22. Set the parallel control to $kp = 0.00006$, and $ki = 0.00002$. Set the parallel power feedback control to $kp = 0.0004$, and $ki = 0.00012$. The dynamic response characteristics based on the different control methods are shown in Figures 17–20.

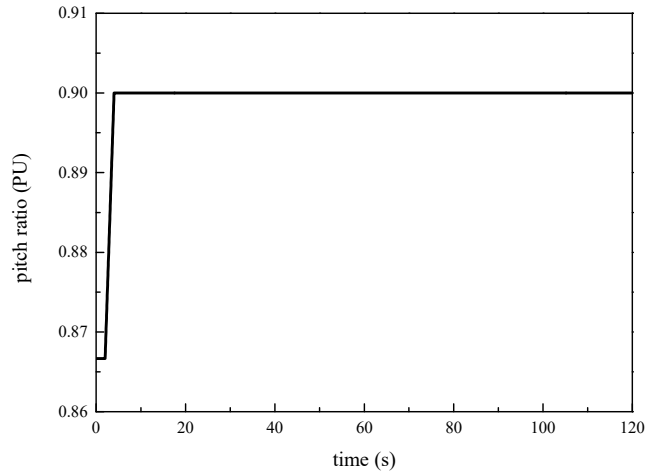


Figure 17. Dynamic characteristics of pitch ratio in the acceleration of COGOG pattern.

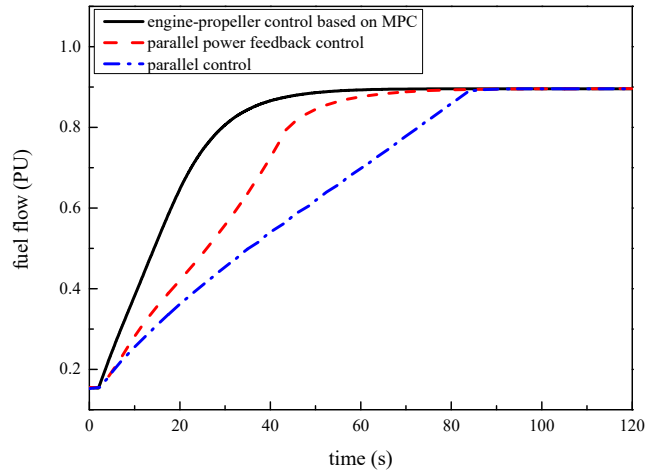


Figure 18. Dynamic characteristics of fuel flow in the acceleration of COGOG pattern.

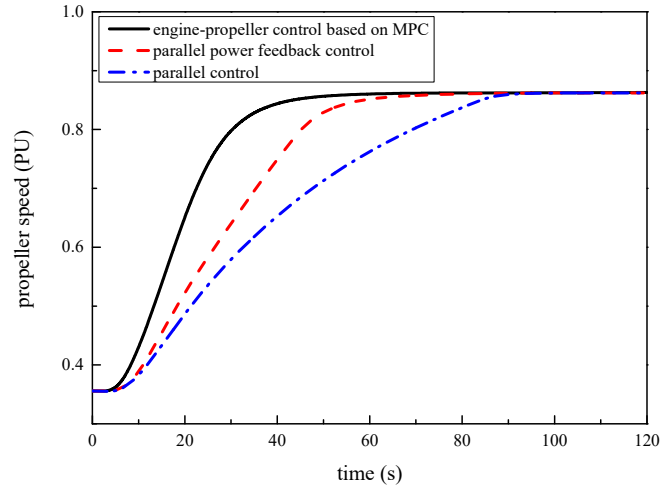


Figure 19. Dynamic characteristics of propeller speed in the acceleration of COGOG pattern.

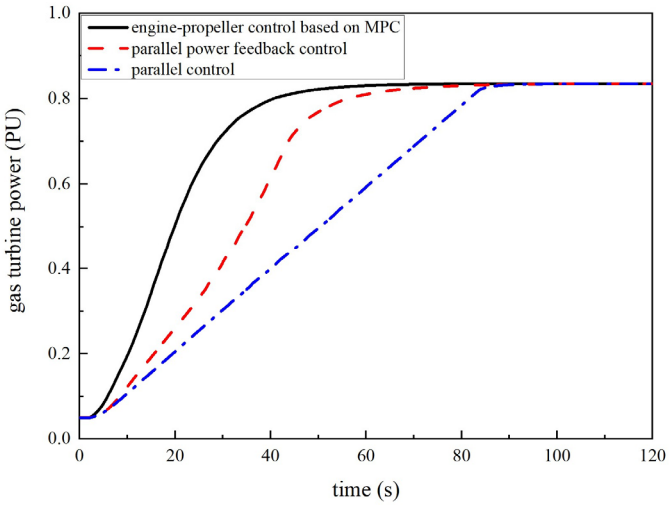


Figure 20. Dynamic characteristics of gas turbine power in the acceleration of COGOG pattern.

In the acceleration process from working condition 1 to working condition 8, it takes about 60 s for propeller speed to reach the target under DNN-MPC control, which is 12 s shorter than the parallel power feedback control. It takes about 88 s for propeller speed to reach the target under parallel control. Compared with the other two control methods, the system under DNN-MPC control has a faster response speed when the acceleration instruction is given. The influence of pitch ratio change on propeller speed is not considered in the two control methods. Meanwhile, the control method based on PID needs to control the fuel flow based on the current and historical deviation, which may lead to lagging regulation. DNN-MPC is based on the deviation between the predicted trajectory and the reference trajectory, and the regulation rule of pitch ratio is added to the optimization objective function, so the prediction model can predict the effect of the change in pitch ratio on propeller speed, so as to accelerate the adjustment speed of fuel flow. The COGOG pattern of the system under DNN-MPC control has better maneuverability.

To verify the robustness of the DNN-MPC control algorithm, the following operations are carried out. Firstly, during the entire acceleration process, random white noise is added to all parameters input into the control algorithm. Then, at 10 s and 30 s, the power turbine speed collection faults are simulated. The collected speed has a significant deviation from the actual speed (At 10 s, the collected speed suddenly increased. At 30 s, the speed collected suddenly dropped). The dynamic response characteristics of the system are shown in Figures 21–23. Whether in the case of random white noise or large-scale disturbances, the DNN-MPC can effectively control the system. As the target variable, the speed changes smoothly in the whole dynamic process. To ensure that the speed can follow the reference state well, there will be sudden changes in the fuel flow. At 10 s, the gas turbine speed suddenly increases, and the fuel flow decreases. Then, the fuel flow immediately resumed the normal trajectory. At 30 s, when the speed is close to the target state, the collected speed suddenly decreases, and the fuel flow increases. However, since the DNN-MPC can predict the future development trajectory of the system, the fuel flow will be quickly adjusted back, so there is no obvious overshoot in the speed. DNN-MPC has been proven to have good robustness.

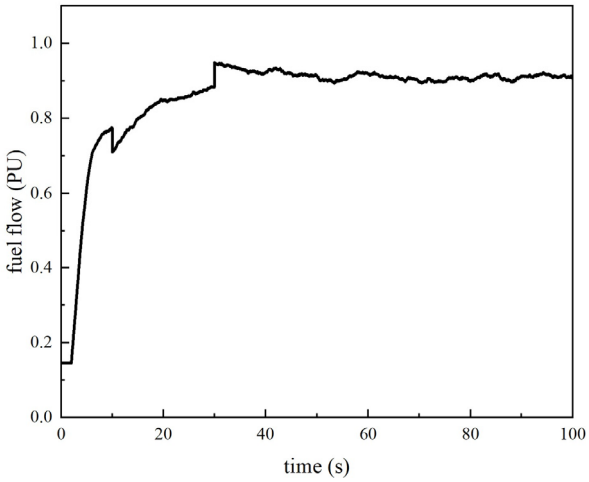


Figure 21. Dynamic characteristics of fuel flow with disturbances.

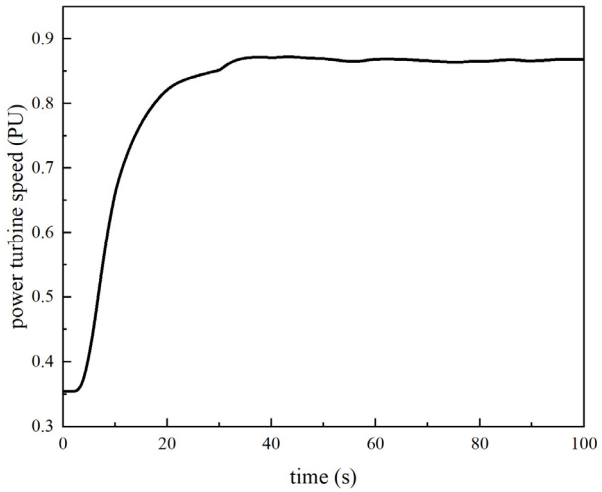


Figure 22. Dynamic characteristics of propeller speed with disturbances.

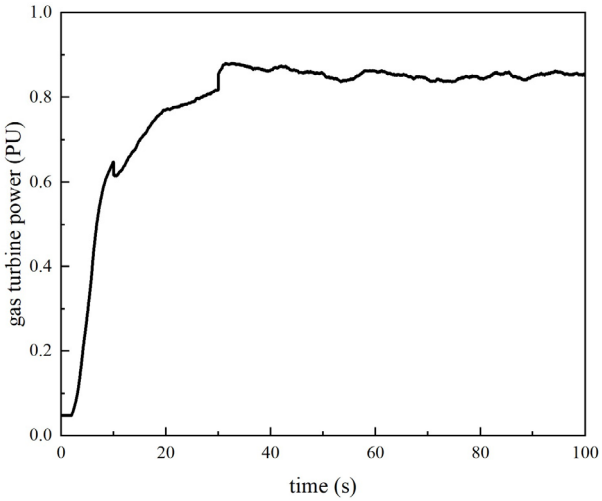


Figure 23. Dynamic characteristics of gas turbine power with disturbances.

Using similar operating conditions to the acceleration process, the deceleration processes from working conditions 8 to 1 under the different control methods are simulated, which are shown in Figures 24–27. In the deceleration process, it takes about 70 s for propeller speed to reach the target and stabilize under DNN-MPC control, which is 22 s

shorter than the parallel power feedback control. It takes about 118 s for propeller speed to reach the target under parallel control. Although the propeller speed based on DNN-MPC control has a small overshoot, it has obvious advantages in terms of dynamic response speed and the time to stabilization. When the deceleration command is given, the propeller speed under DNN-MPC control will decrease rapidly, while the propeller speed under the other two control methods will rise first and then decrease, which is caused by the decrease in pitch ratio. As the pitch decreases, the contact area between the blade and the water flow decreases, resulting in a rapid reduction in propeller torque. At this time, the gas turbine power under the other two control methods decreases slowly, resulting in the active torque being greater than the loaded torque, so the propeller speed increases. Since the prediction model can predict the impact of reduced pitch ratio on propeller speed, DNN-MPC can accelerate the adjustment of fuel flow so that the propeller speed controlled by DNN-MPC does not increase. The superiority of the engine-propeller cooperative control is demonstrated.

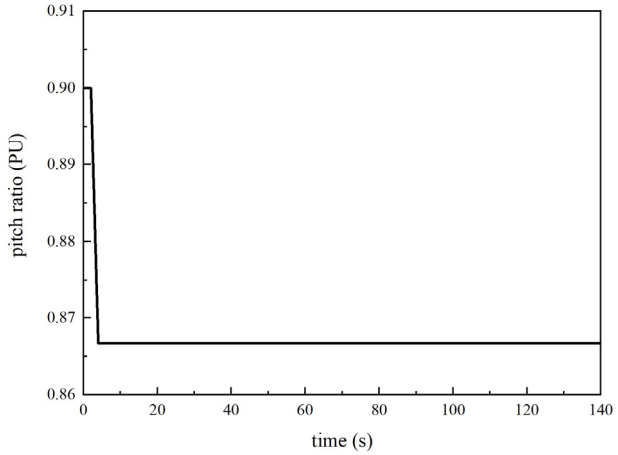


Figure 24. Dynamic characteristics of pitch ratio in the deceleration of COGOG pattern.

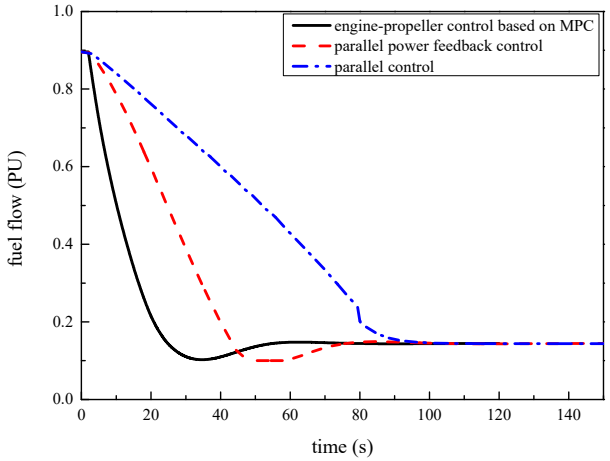


Figure 25. Dynamic characteristics of fuel flow in the deceleration of COGOG pattern.

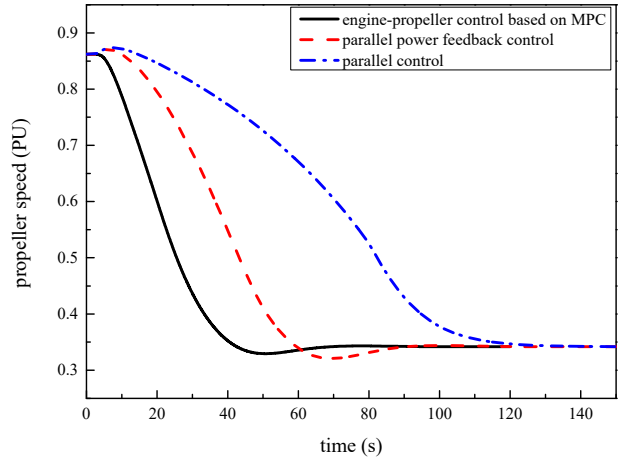


Figure 26. Dynamic characteristics of propeller speed in the deceleration of COGOG pattern.

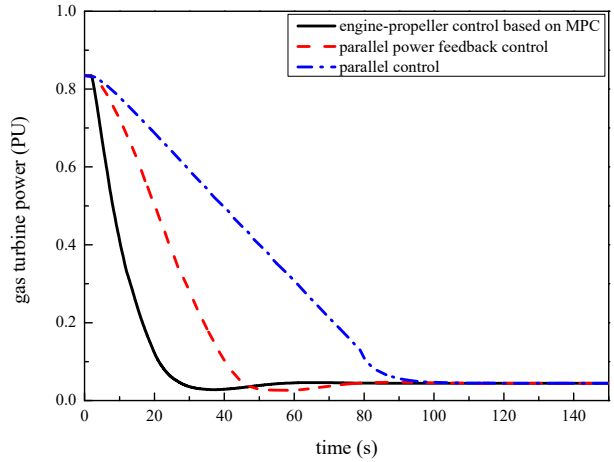


Figure 27. Dynamic characteristics of gas turbine power in the deceleration of COGOG pattern.

4.2. Power Distribution Control

The power distribution process is simulated under working condition 8 when the COGOG pattern switches to the COGAG pattern. The operating conditions are as follows. In the first 2 s, the system runs stably at working condition 8, when 1#GT provides almost all the power for the propeller, and 2#GT only provides a small amount of power. At 2 s, the power distribution command is given to make the two gas turbines provide the same power to the propeller. The simulation finishes at 80 s. Set the weight factor of MPC to $\Gamma_{y,2n-1} = 0.78$, $\Gamma_{y,2n} = 0.82$, $\Gamma_{u,2n-1} = 0.22$, and $\Gamma_{u,2n} = 0.18$. Set the parallel control to $kp = 0.00008$, and $ki = 0.00006$. Set the parallel power feedback control to $kp = 0.0002$, $ki = 0.00002$, $kp_s = 0.04$, and $kp_p = 0.06$. The dynamic response characteristics based on the different control methods are shown in Figures 28–31.

In the power distribution process, it takes about 27 s for power balance under DNN-MPC control. It takes about 32 s under parallel power feedback control and about 50 s under parallel control. The power distribution speed under DNN-MPC control is the fastest, and it takes the least time for fuel flow and gas turbine power to reach equilibrium. The parallel control method takes gas turbine power as the control target variable. Since the rate of power increase is fixed, the more power that is distributed, the longer it takes. Under parallel power feedback control and DNN-MPC control, the greater the difference between the current power and target power, the faster the power distribution is. As the power approaches the target, the slope of the power curve gradually flattens. The fluctuation of propeller speed under parallel control is the smallest, but the stabilization speed is the

slowest. It takes the shortest time to stabilize the propeller speed under DNN-MPC control, about 32 s. The COGAG system under DNN-MPC control shows the best maneuverability in both power distribution and propeller speed stabilization.

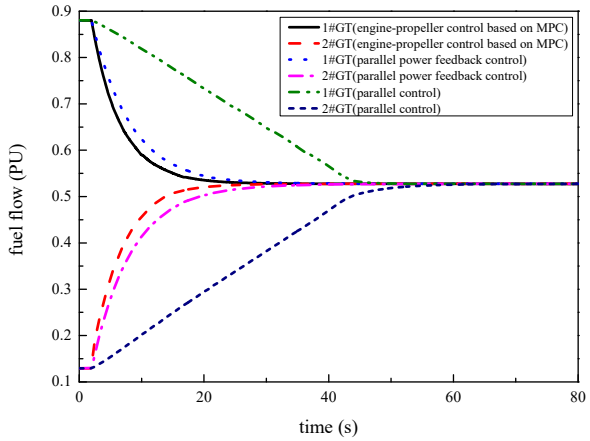


Figure 28. Dynamic characteristics of fuel flow in the power distribution process.

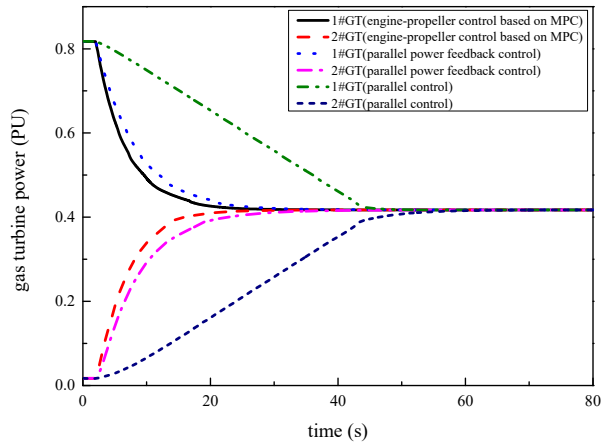


Figure 29. Dynamic characteristics of gas turbine power in the power distribution process.

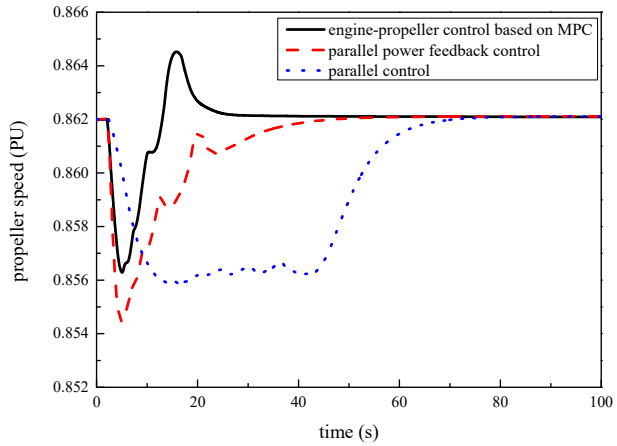


Figure 30. Dynamic characteristics of propeller speed in the power distribution process.

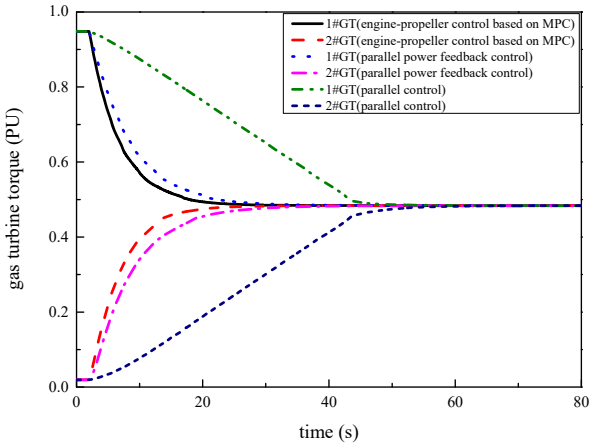


Figure 31. Dynamic characteristics of gas turbine torque in the power distribution process.

The power transfer process is simulated under working condition 8 when the COGAG pattern switches to the COGOG pattern, which is the reverse of the power distribution. The dynamic response characteristics based on the different control methods are shown in Figures 32–35.

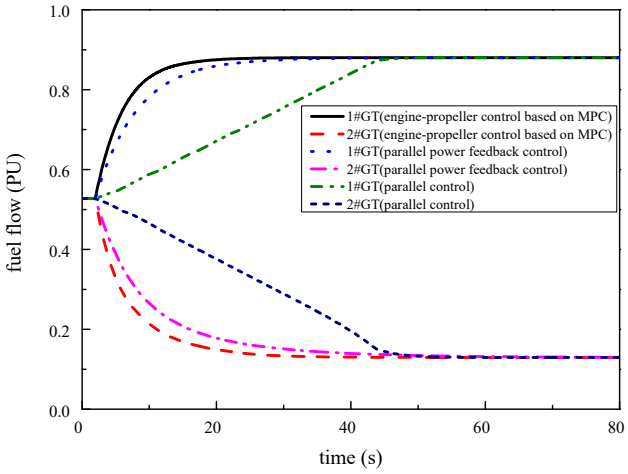


Figure 32. Dynamic characteristics of fuel flow in the power transfer process.

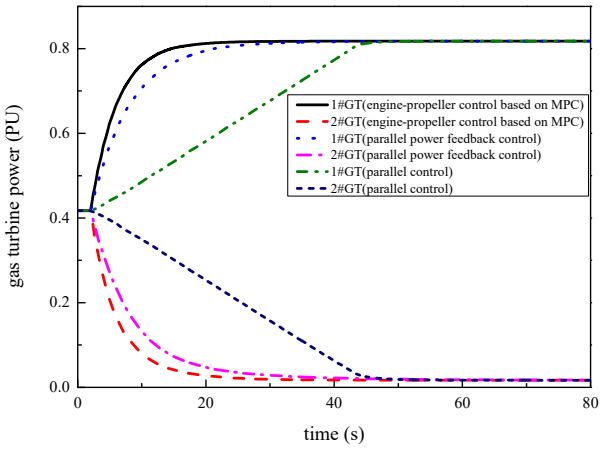


Figure 33. Dynamic characteristics of gas turbine power in the power transfer process.

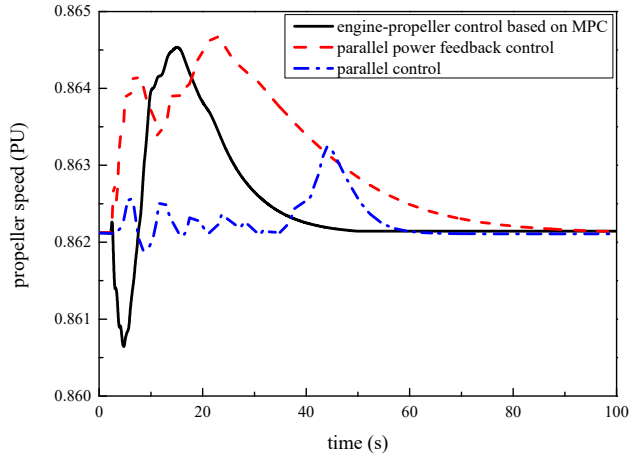


Figure 34. Dynamic characteristics of propeller speed in the power transfer process.

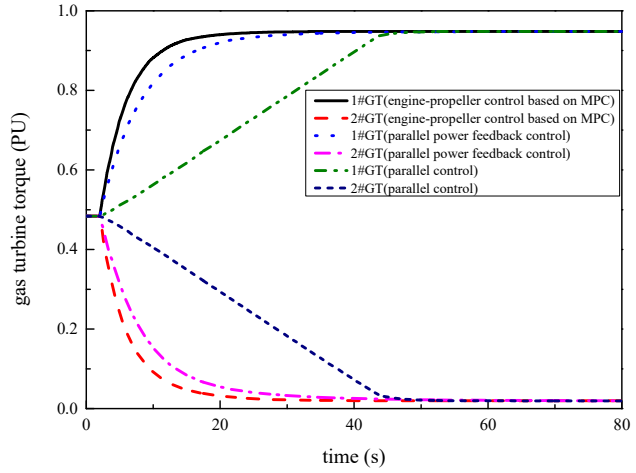


Figure 35. Dynamic characteristics of gas turbine torque in the power transfer process.

In the power transfer process, it takes about 30 s for power stabilization under DNN-MPC control. It takes about 37 s under parallel power feedback control and about 43 s under parallel control. Fuel flow and gas turbine power based on DNN-MPC control take the shortest time to reach stability. Because the power transfer rate of the two gas turbines under parallel control is the same, the power transfer time is longer than that of the other two methods. It is also for that reason that propeller speed under parallel control has the smallest fluctuation. It takes the shortest time to stabilize propeller speed under DNN-MPC control, about 46 s, which is 10 s shorter than that under parallel control. It takes about 80 s for propeller speed stabilization under parallel power feedback control. In the process of power distribution and power transfer, no overshoot occurs in fuel flow and power, and there is no steady-state error in power either.

4.3. Speed Control in the COGAG Pattern

The acceleration process of the system under the COGAG pattern from working conditions 1 to 10 is simulated. The operating conditions are as follows. In the first 2 s, the system runs at working condition 1. At 2 s, the acceleration command is given to accelerate the system to working condition 10. The simulation finishes at 120 s. Set the weight factor of MPC to $\Gamma_{y,n}$ = 0.78, $\Gamma_{u,n}$ = 0.22, and $\Gamma_{b,n}$ = 0.78. Set the parallel control to $kp = 0.00006$, and $ki = 0.00003$. Set the parallel power feedback control to $kp = 0.0004$, $ki = 0.00002$, $kp_s = 0.38$, and $kp_p = 0.38$. The dynamic response characteristics based on the different control methods are shown in Figures 36–39.

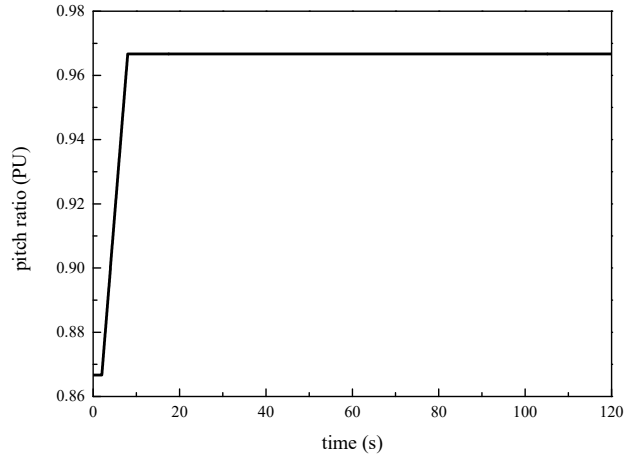


Figure 36. Dynamic characteristics of pitch ratio in the acceleration of COGAG pattern.

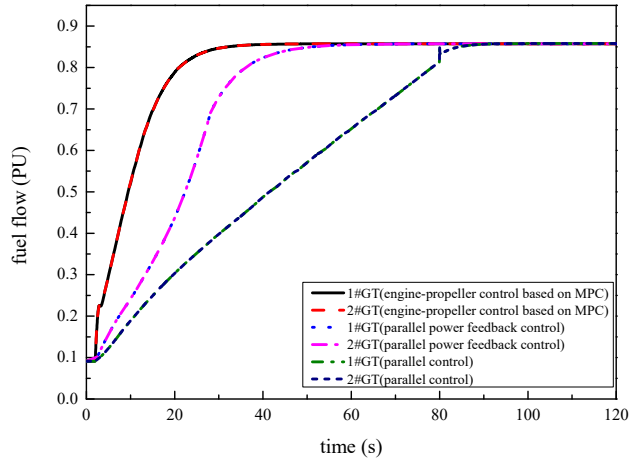


Figure 37. Dynamic characteristics of fuel flow in the acceleration of COGAG pattern.

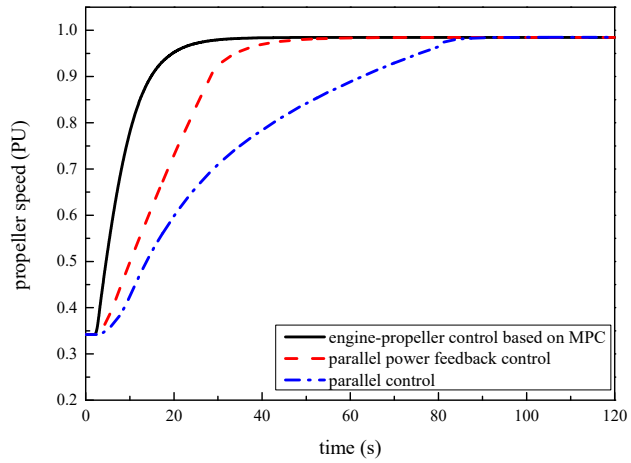


Figure 38. Dynamic characteristics of propeller speed in the acceleration of COGAG pattern.

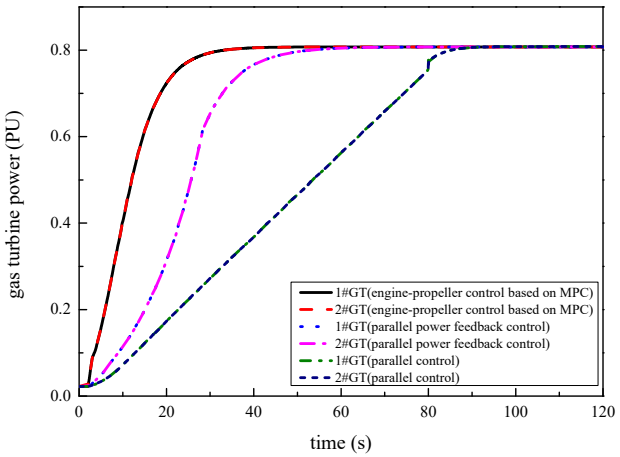


Figure 39. Dynamic characteristics of gas turbine power in the acceleration of COGAG pattern.

In the acceleration process from working conditions 1 to 10, the pitch ratio increased linearly from 0.867 to 0.967. It takes about 40 s for propeller speed to reach the target under DNN-MPC control, which is 12 s shorter than parallel power feedback control. It takes about 80 s for propeller speed to reach the target under parallel control. In the initial stage of acceleration, the fuel flow under DNN-MPC control is adjusted more quickly, and propeller speed rises the fastest. As propeller speed approaches the target, the speed curve gradually flattens, and there is no overshoot. The curves of the fuel flow and power of the two gas turbines basically coincide under DNN-MPC control, which shows that the two gas turbines have good synchronization performance. The other two control methods do not consider the influence of pitch ratio on propeller speed, so the change in pitch ratio does not affect the adjustment speed of fuel flow. In fact, the adjustment rate of fuel flow under parallel power feedback control and DNN-MPC control within 15–25 s is relatively close. Since DNN-MPC control takes into account the engine-propeller matching characteristics, the fuel flow regulation speed is faster than that of the parallel power feedback control in the initial stage of acceleration. Meanwhile, as the propeller speed approaches the target, the fuel flow regulation under parallel power feedback control becomes slow. Therefore, the dynamic performance of the system under engine-propeller cooperative control based on DNN-MPC is better.

Using similar operating condition to the acceleration process, the deceleration processes from working conditions 10 to 1 under the different control methods are simulated, which are shown in Figures 40–43. In the deceleration process, it takes about 53 s for propeller speed to reach the target under DNN-MPC control, which is 27 s shorter than parallel power feedback control. It takes about 108 s for propeller speed to reach the target under parallel control. The COGAG system under DNN-MPC control shows the best dynamic performance. When the deceleration instruction is given, the propeller speed under the other two control methods will first increase and then decrease, which is also caused by the reduction in pitch ratio. The propeller speed increase is more obvious under parallel control. Parallel power feedback control takes the propeller speed as the control target. The larger the difference between the actual speed and the target, the faster the fuel flow adjustment speed, which alleviates the amplitude of the propeller speed rising. Due to the good predictability of DNN-MPC control, it can speed up fuel flow regulation to prevent the propeller speed from increasing. Moreover, no overshot occurs in fuel flow, propeller speed, and power. In engineering practice, in order to avoid over-rotation caused by rising propeller speed, the pitch ratio is generally adjusted when the propeller speed is reduced to a certain range. Under engine-propeller cooperative control based on DNN-MPC, the pitch adjustment can be operated directly. In addition, the computational efficiency of the

DNN-MPC algorithm needs to be verified. The hardware configuration of the computer is as follows: CPU i5-4460S @ 2.90 GHz, memory 4 GB. Running the DNN-MPC algorithm based on the Python environment, in a single sampling period, the average calculation time of the prediction model is approximately 22.8 ms, and the average time consumption of the optimization solution algorithm is approximately 3 ms. Since the essence of DNN-MPC still belongs to linear MPC, it has better computational efficiency.

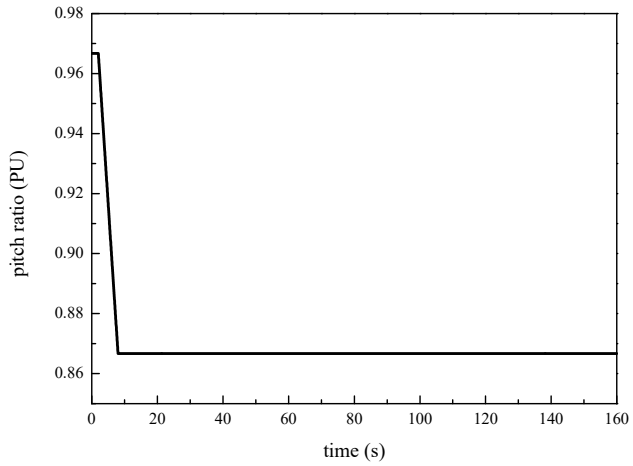


Figure 40. Dynamic characteristics of pitch ratio in the deceleration of COGAG pattern.

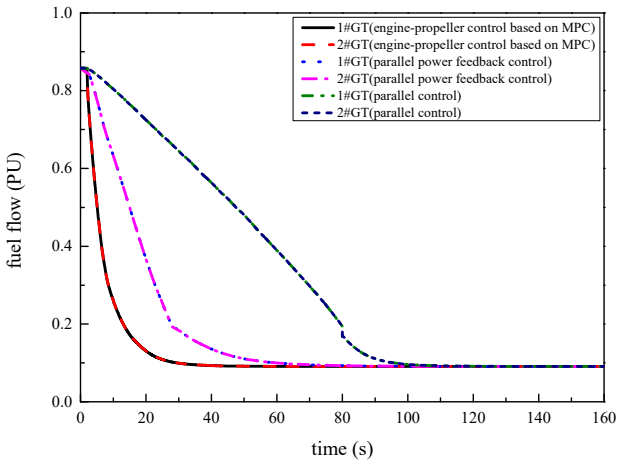


Figure 41. Dynamic characteristics of fuel flow in the deceleration of COGAG pattern.

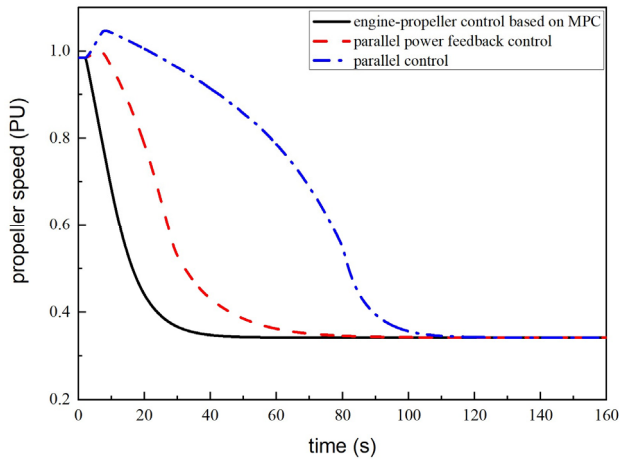


Figure 42. Dynamic characteristics of propeller speed in the deceleration of COGAG pattern.

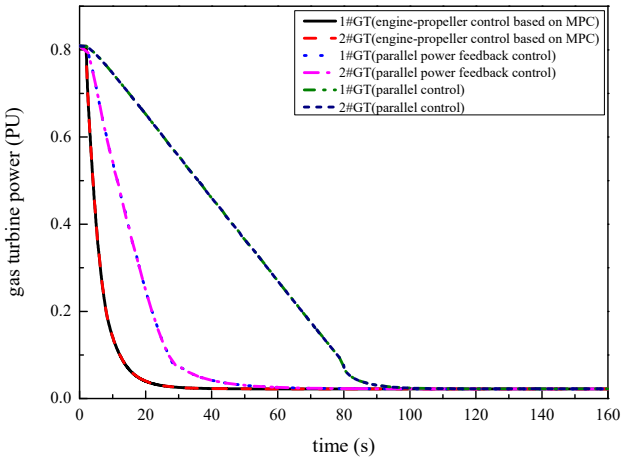


Figure 43. Dynamic characteristics of gas turbine power in the deceleration of COGAG pattern.

5. Conclusions

The COGAG system is a common power plant for large vessels. Under the existing control methods, the steady-state and dynamic characteristics of the COGAG system have a large space for improvement. In this paper, a multi-objective optimal control method is proposed to improve economy, maneuverability, and stability. In essence, DNN-MPC belongs to linear model predictive control, so it has advantages in computational efficiency compared with nonlinear model predictive control. The following conclusions can be summarized.

1. The fuel consumption per nautical mile for evaluating the economy of the COGAG system is proposed. Based on the complete nonlinear model, the ship engine-propeller matching characteristics under different operating patterns are studied. The economic optimization operation strategy is formulated.
2. A two-layer control method is proposed for the COGAG system. The economic optimization operation strategy is put into the system planning layer. When the vessel speed command is given, the optimal operation point can be identified to improve economy. When the vessel runs in 10th gear, the economic efficiency of the optimized COGAG system can reach 22.47%. Taking the optimal operation point as the reference state and putting it into the local control layer, the engine-propeller cooperative control is designed to improve maneuverability.
3. Considering that COGAG system has a short sampling and control period, and the operation range of the system is large, a deep neural network (DNN) model with an LPV form is proposed as the prediction model. The DNN model has high accuracy which can be entirely equivalent to the complete nonlinear model. Moreover, the DNN model has the ability of ultra-real-time operation.
4. The engine-propeller cooperative control based on DNN-MPC is proposed for different dynamic processes of the COGAG system. Compared with parallel control based on PI and parallel power feedback control based on PID, the DNN-MPC control can significantly improve the maneuverability of the COGAG system and avoid propeller speed overshoot caused by pitch adjustment. Compared with the PID-based control, the DNN-MPC control can improve the maneuverability of the COGOG pattern by 31.82% and 16.67% in the process of accelerating from 1st to 8th gear and improve the maneuverability of the COGAG pattern by 50% and 23.08% in the process of accelerating from 1st to 10th gear. Under DNN-MPC control, the gas turbines show good synchronization performance, which means that the stability of the COGAG system can be guaranteed.

5. The proposed multi-objective optimization control method is suitable for the power plant which includes multiple power sources. The control algorithm needs to be optimized based on the performance requirements of the specific device. Considering that performance degradation can change the economic optimization operation strategy, a degradation identification and strategy update method will be studied in the future. In addition, theory on the control stability of combining neural networks with MPC is also an important research area.

Author Contributions: Conceptualization, X.L.; methodology, J.Z. and J.L.; software, J.Z.; validation, J.Z. and J.L.; formal analysis, J.Z.; investigation, J.Z.; resources, X.L.; data curation, J.Z. and J.L.; writing—original draft preparation, J.Z. and J.L.; writing—review and editing, X.L.; visualization, J.Z. and J.L.; supervision, X.M. and X.L.; project administration, X.L. All authors have read and agreed to the published version of the manuscript.

Funding: This research received no external funding.

Data Availability Statement: Because the research object and data of this manuscript are sensitive, the data sets used and analyzed during the current study are available from the corresponding author on reasonable request.

Acknowledgments: The authors would like to thank the Editor-in-Chief, Associate Editor, and anonymous referees for their invaluable comments and suggestions.

Conflicts of Interest: The authors declare that they have no known competing financial interests or personal relationships that could have appeared to influence the work reported in this paper.

References

1. Wang, Z.; Ma, J.; Yu, H.; Li, T. Research on Matching Characteristics of Ship-Engine-Propeller of COGAG. In Proceedings of the ASME Turbo Expo 2021, Virtual, Online, 7–11 June 2021. [CrossRef]
2. Xu, Z.; Wen, X.; Zhao, N. A Novel COGAG Propulsion System for Marine Ships. In Proceedings of the ASME Turbo Expo 2018, Oslo, Norway, 11–15 June 2018. [CrossRef]
3. Altosole, M.; Benvenuto, G.; Figari, M.; Campora, U. Real-time simulation of a COGAG naval ship propulsion system. *Proc. Inst. Mech. Eng. Part M J. Eng. Marit. Environ.* **2009**, *223*, 47–62. [CrossRef]
4. Xie, C.; Wang, Z. The Research on Merging Control Strategy of COGAG Power Plant. *Adv. Mater. Res.* **2011**, *159*, 297–302. [CrossRef]
5. Li, Z.; Li, S.; Cao, Y.; Li, D. Study and Design of COGAG Controller. In Proceedings of the 2012 Second International Conference on Instrumentation, Measurement, Computer, Communication and Control, Harbin, China, 8–10 December 2012. [CrossRef]
6. Li, T.; Wang, Z.; Li, S. Simulation of performance characteristics of a combined gas turbine and gas turbine device. *Harbin Gongcheng Daxue Xuebao* **2016**, *37*, 1366–1372. [CrossRef]
7. Meng, H.; Wang, Z.; Li, S.; Zhao, N.; Jin, G. The Simulation Study on Dynamic Characteristics of COGAG Engaging Process. *Adv. Mater. Res.* **2014**, *960–961*, 1442–1445. [CrossRef]
8. Ma, Y.; Liu, J.; Li, Q.; Liu, H.; Yu, D. Three-Spool Marine Gas Turbine Multi-Objective Switching Control System Design and Optimization. *IFAC-PapersOnLine* **2021**, *54*, 388–393. [CrossRef]
9. Chen, C.; Long, L.; Mao, X.; Li, L. A Multi-objective Switching Control Strategy for Aero-engines Considering Sensor Dynamic. In Proceedings of the 31st Chinese Control and Decision Conference, Nanchang, China, 3–5 June 2019. [CrossRef]
10. Ma, Y.; Liu, J.; Zhu, L.; Li, Q.; Liu, H.; Yu, D. Accommodation of Multishaft Gas Turbine Switching Control Gain Tuning Problem to Inlet Guide Vane Position. *J. Eng. Gas Turbines Power* **2022**, *144*, 031014. [CrossRef]
11. Fan, L.; Shen, C.; Lu, Z.; Xu, C.; Wang, Z.; Ma, X. Multi-objective Optimization of Three-shaft Gas Turbine for Sudden Unloading. *IFAC-PapersOnLine* **2021**, *54*, 400–405. [CrossRef]
12. Yan, P.; Zhang, Z.; Lei, X.; Hou, Q.; Wang, H. A multi-objective optimal control model of cascade pumping stations considering both cost and safety. *J. Clean. Prod.* **2022**, *345*, 131171. [CrossRef]
13. Han, Y.; Zhang, G.; Li, Q.; You, Z.; Chen, W.; Liu, H. Hierarchical energy management for PV/hydrogen/battery island DC microgrid. *Int. J. Hydrog. Energy* **2019**, *44*, 5507–5516. [CrossRef]
14. Pu, Y.; Li, Q.; Chen, W.; Liu, H. Hierarchical energy management control for islanding DC microgrid with electric-hydrogen hybrid storage system. *Int. J. Hydrog. Energy* **2019**, *44*, 5153–5161. [CrossRef]

15. Wang, J.; Han, H.; Yang, Y.; Wei, M. An improved model predictive control approach for fuel efficiency optimization of vessel propulsion systems. *Control Eng. Pract.* **2021**, *109*, 104749. [CrossRef]
16. Mei, D.; Wang, G.; Ye, Z.; Shen, J.; Feng, H. Two-layer Optimization Method of Vessel Power System Structure Performance Based on Variable-order Genetic Algorithm. *Zhongguo Dianji Gongcheng Xuebao* **2018**, *38*, 5763–5771. [CrossRef]
17. Carreño, J.E.; Mora, J.D.; Pérez, F.L. Mathematical model for maneuverability of a riverine support patrol vessel with a pump-jet propulsion system. *Ocean Eng.* **2013**, *63*, 96–104. [CrossRef]
18. Gutiérrez-Urquídez, R.C.; Valencia-Palomo, G.; Rodríguez-Elias, O.M.; Trujillo, L. Systematic selection of tuning parameters for efficient predictive controllers using a multiobjective evolutionary algorithm. *Appl. Soft Comput. J.* **2015**, *31*, 326–338. [CrossRef]
19. Chen, H.; Li, Q.; Ye, Z.; Pang, S. Neural Network-Based Parameter Estimation and Compensation Control for Time-Delay Servo System of Aeroengine. *Aerospace* **2025**, *12*, 64. [CrossRef]
20. Vroemen, B.; Van Essen, H.; Van Steenhoven, A.; Kok, J. Nonlinear model predictive control of a laboratory gas turbine installation. In Proceedings of the ASME 1998 International Gas Turbine and Aeroengine Congress and Exhibition, Stockholm, Sweden, 2–5 June 1998. [CrossRef]
21. Surendran, S.; Chandrawanshi, R.; Kulkarni, S.; Bhartiya, S.; Nataraj Paluri, S.; Sampath, S. Model predictive control of a laboratory gas turbine. In Proceedings of the 2016 Indian Control Conference, Hyderabad, India, 4–6 January 2016. [CrossRef]
22. Zhou, X.; Lu, F.; Zhou, W.; Huang, J. An improved multivariable generalized predictive control algorithm for direct performance control of gas turbine engine. *Aerosp. Sci. Technol.* **2020**, *99*, 105576. [CrossRef]
23. Vahab, H.H.; Afef, F.; Concepción, A.M.; Ramin, F.A. Adaptive model predictive control design for the speed and temperature control of a V94.2 gas turbine unit in a combined cycle power plant. *Energy* **2020**, *207*, 118259. [CrossRef]
24. Hou, G.; Gong, L.; Huang, C.; Zhang, J. Fuzzy modeling and fast model predictive control of gas turbine system. *Energy* **2020**, *200*, 117465. [CrossRef]
25. Valencia-Palomo, G.; Rossiter, J.A.; López-Estrada, F.R. Improving the feed-forward compensator in predictive control for setpoint tracking. *ISA Trans.* **2014**, *53*, 755–766. [CrossRef]
26. Hassan, A.; Ruiz-Moreno, S.; Frejo, J.R.D.; Maestre, J.M.; Camacho, E.F. Neural-Network Based MPC for Enhanced Lateral Stability in Electric Vehicles. *IEEE Access* **2024**, *12*, 23265–23278. [CrossRef]
27. Jin, L.; Liu, L.; Wang, X.; Shang, M.; Wang, F.-Y. Physical-Informed Neural Network for MPC-Based Trajectory Tracking of Vehicles With Noise Considered. *IEEE Trans. Intell. Veh.* **2024**, *9*, 4493–4503. [CrossRef]
28. Wen, J.; Lu, J.; Spataru, C.; Weng, Y.; Lv, X. Coordinated intelligent control strategy and power management for marine gas turbine under pulsed load using optimized neural network. *Energy* **2024**, *313*, 133719. [CrossRef]
29. Dang, T.; Debrouwere, F.; Hostens, E. Approximating Nonlinear Model Predictive Controllers using Support Vector Machines. In Proceedings of the Australian & New Zealand Control Conference, Gold Coast, Australia, 25–26 November 2021. [CrossRef]
30. Liu, Z.; Karimi, I.A. Gas turbine performance prediction via machine learning. *Energy* **2020**, *192*, 116627. [CrossRef]
31. Wang, C.; Zhang, L. Control oriented fast optimisation with SHapley additive explanations assisted two-stage training of input convex neural network. *Eng. Appl. Artif. Intell.* **2025**, *151*, 110625. [CrossRef]
32. Gan, W.; Zhu, D.; Ji, D. QPSO-model predictive control-based approach to dynamic trajectory tracking control for unmanned underwater vehicles. *Ocean Eng.* **2018**, *158*, 208–220. [CrossRef]
33. Tian, Z.; Li, S.; Wang, Y.; Wang, X. SVM Predictive Control for Calcination Zone Temperature in Lime Rotary Kiln with Improved PSO Algorithm. *Trans. Inst. Meas. Control* **2018**, *40*, 3134–3146. [CrossRef]
34. Shamma, J.; Athans, M. Guaranteed properties of gain scheduled control for linear parameter varying plants. *Automatica* **1991**, *27*, 559–564. [CrossRef]
35. Lv, C.; Lan, Z.; Wang, Z.; Chang, J.; Yu, D. Intelligent ammonia precooling control for TBCC mode transition based on neural network improved equilibrium manifold expansion model. *Energy* **2024**, *288*, 129662. [CrossRef]
36. Lyu, C.; Chang, J.; Yu, D. Feedback Linearized Sliding Mode Control of Turbofan Engine Based on Multiple Input Multiple Output Equilibrium Manifold Expansion Model. *Tuijin Jishu* **2021**, *42*, 1681–1689.
37. Zhu, L.; Liu, J.; Zhou, W.; Yu, D. An Improvement Method Based on Similarity Theory for Equilibrium Manifold Expansion Model. In Proceedings of the 2019 IEEE International Conference Power Data Science, Taizhou, China, 12–15 December 2019; IEEE: New York, NY, USA, 2019.
38. Zhu, L.; Liu, J.; Ma, Y.; Zhou, W.; Yu, D. A corrected equilibrium manifold expansion model for gas turbine system simulation and control. *Energies* **2020**, *13*, 4904. [CrossRef]
39. Lv, C.; Lan, Z.; Chang, J.; Yu, D. Adaptive dynamic programming for ramjet intelligent tracking control via neural network-enhanced equilibrium manifold expansion estimator. *Energy* **2024**, *309*, 133905. [CrossRef]
40. Li, T.; Liu, R.; Wang, Z.; Zhou, S.; Zhang, J.; Gao, C. Integrated simulation and optimization matching methods of intercooled gas turbi-nes. *Harbin Gongcheng Daxue Xuebao* **2021**, *42*, 1195–1202. [CrossRef]
41. Kim, T.; Hwang, S. Part load performance analysis of recuperated gas turbines considering engine configuration and operation strategy. *Energy* **2006**, *31*, 260–277. [CrossRef]

42. Yu, Y.; Chen, L.; Sun, F.; Wu, C. Matlab/Simulink-based simulation for digital-control system of marine three-shaft gas-turbine. *Appl. Energy* **2005**, *80*, 1–10. [CrossRef]
43. Li, J.; Wang, Z.; Li, S. Design and Simulation of MPC for Marine Three-shaft Gas Turbine. *IFAC-PapersOnLine* **2021**, *54*, 382–387. [CrossRef]
44. Lotfi, F.; Virji, K.; Faraji, F.; Berry, L.; Holliday, A.; Meger, D.; Dudek, G. Uncertainty-aware hybrid paradigm of nonlinear MPC and model-based RL for offroad navigation: Exploration of transformers in the predictive model. In Proceedings of the IEEE International Conference on Robotics and Automation, Yokohama, Japan, 13–17 May 2024. [CrossRef]
45. Ma, S.; Ding, J. Multi-model based MPC to improve the ramp rate for renewable energy consumption. *Neurocomputing* **2025**, *611*, 128619. [CrossRef]
46. Li, J.; Wang, Z.; Li, S.; Ming, L. A SDNN-MPC method for power distribution of COGAG propulsion system. *Energy* **2022**, *254*, 124310. [CrossRef]
47. Liu, S.; Wang, J. A simplified dual neural network for quadratic programming with its KWTA application. *IEEE Trans. Neural Netw.* **2006**, *17*, 1500–1510. [CrossRef]

Disclaimer/Publisher's Note: The statements, opinions and data contained in all publications are solely those of the individual author(s) and contributor(s) and not of MDPI and/or the editor(s). MDPI and/or the editor(s) disclaim responsibility for any injury to people or property resulting from any ideas, methods, instructions or products referred to in the content.